Åbo Akademi University

Wenyang Xu

Three-dimensional printing of wood-derived biopolymers towards biomedical applications

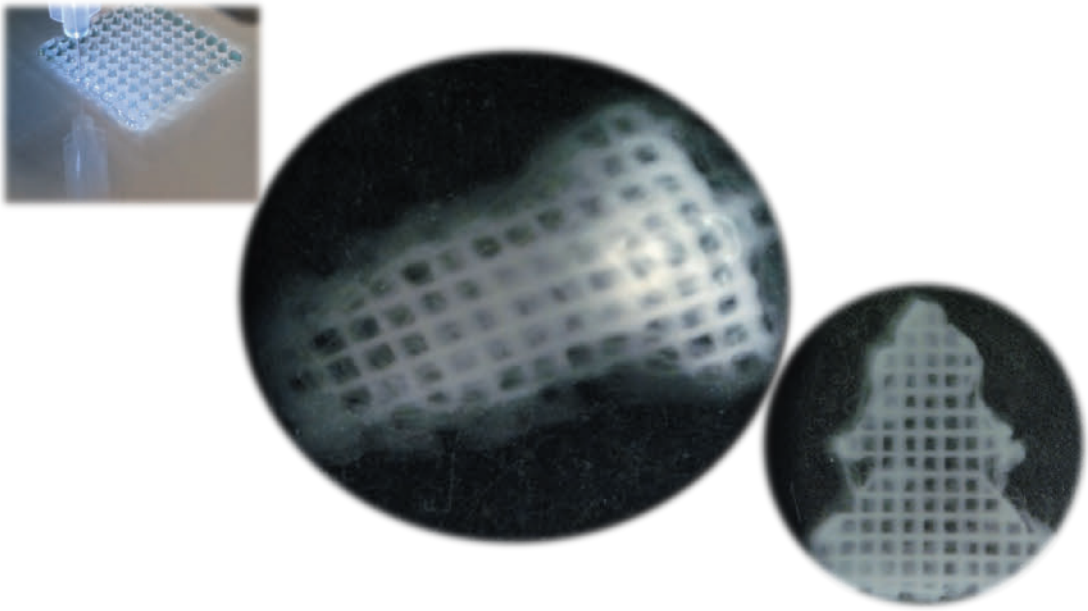

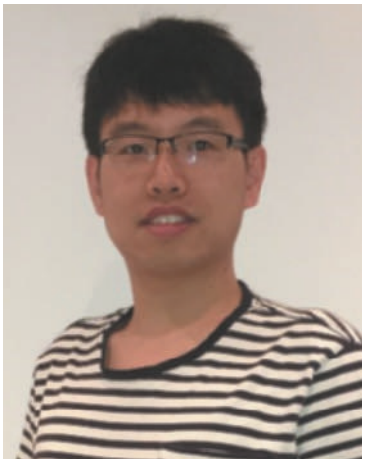

Wenyang Xu

Born 1991, Qingdao, Shandong, P.R. China

B.Sc. Light Industry and Chemical Engineering (Pulping and Papermaking), 2013
Qilu University of Technology, Jinan, Shandong, China

M.Sc. Chemical Engineering, 2015
Åbo Akademi University, Turku/Åbo, Finland

Ph.D. studies at the Laboratory of Wood and Paper Chemistry from June of 2015
Åbo Akademi University, Turku/Åbo, Finland

Three-dimensional printing of wood-derived biopolymers towards biomedical applications

Wenyang Xu

Laboratory of Wood and Paper Chemistry
Johan Gadolin Process Chemistry Centre
Faculty of Science and Engineering
Åbo Akademi University
Turku/Åbo, Finland, 2019

Supervisors:
Adjunct Professor Chunlin Xu
Laboratory of Wood and Paper Chemistry
Johan Gadolin Process Chemistry Centre
Åbo Akademi University
Åbo, Finland

Professor Stefan Willför
Laboratory of Wood and Paper Chemistry
Johan Gadolin Process Chemistry Centre
Åbo Akademi University
Åbo, Finland

Reviewers:
Professor Run-Cang Sun
College of Materials Science and Technology
Beijing Forestry University
Beijing, China

Professor Maija Tenkanen
Department of Food and Nutrition
University of Helsinki
Helsinki, Finland

Opponent:
Professor Run-Cang Sun
College of Materials Science and Technology
Beijing Forestry University
Beijing, China

ISBN 978-952-12-3787-4 (printed)
ISBN 978-952-12-3788-1 (digital)
Painosalama Oy – Turku, Finalnd 2019

To Xue and Edwin

To the family

Contents

Preface

List of publications

I **Wenyang Xu,** Xiaoju Wang, Niklas Sandler, Stefan Willför, Chunlin Xu. Three-dimensional printing of wood-derived biopolymers: A review focused on biomedical applications. *ACS Sustainable Chemistry & Engineering*, 2018, 6(5), 5663-5680.

II **Wenyang Xu**, Andrey Pranovich, Peter Uppstu, Xiaoju Wang, Dennis Kronlund, Jarl Hemming, Heidi Öblom, Niko Moritz, Maren Preis, Niklas Sandler, Stefan Willför, Chunlin Xu. Novel biorenewable composite of wood polysaccharide and polylactic acid for three dimensional printing. *Carbohydrate Polymers*, 2018, 187, 51-58.

III **Wenyang Xu**, Binbin Zhang Molino, Fang Cheng, Paul J. Molino, Zhilian Yue, Dandan Su, Xiaoju Wang, Stefan Willför, Chunlin Xu, Gordon G. Wallace. On low-Concentration inks formulated by nanocellulose assisted with gelatin methacrylate (GelMA) for 3D printing towards wound healing application. *ACS Applied Materials & Interfaces*, 2018, *under revision.*

IV Kajsa Markstedt, **Wenyang Xu**, Jun Liu, Chunlin Xu, Paul Gatenholm. Synthesis of tunable hydrogels based on O-acetyl-galactoglucomannans from spruce. *Carbohydrate Polymers*, 2017, 157, 1349-1357.

V **Wenyang Xu**, Xue Zhang, Otto Långvik, Xiaoju Wang, Yongchao Zhang, Monika Österberg, Stefan Willför, Chunlin Xu. A surface engineered biomimetic ink formulation based on nanocellulose and UV cross-linkable hemicellulose for 3D printing. *ACS Applied Materials & Interfaces*, 2018, *under revision*.

This work was carried out at the Laboratory of Wood and Paper Chemistry during the years of 2015-2018 under the supervision of Professor Stefan Willför and Adjunct Professor Chunlin Xu at Åbo Akademi University. Part of the work was carried out at the ARC Centre of Excellence for Electromaterials Science, Intelligent Polymer Research Institute, University of Wollongong, Australia.

Contribution of the author

The author of this thesis was responsible for the planning and writing of article **I**. For publication **II**, the author was responsible for the experimental work, and writing of the article. The author was responsible for planning, experimental work, and writing the articles of **III**. In paper **IV**, the author was second-author for the article and participated in practical experiments including synthesis and characterization, and writing of the manuscript. The author was responsible for planning, experimental work, and writing the articles of paper **V** except cell studies.

Supporting publications, proceedings, and presentations

1. Chunlin Xu, Binbin Zhang, Xiaoju Wang, Fang Cheng, **Wenyang Xu**, Paul Molino, Markus Bacher, Dandan Su, Thomas Rosenau, Stefan Willför, Gordon G. Wallace. 3D printing of nanocellulose hydrogel scaffolds with tunable mechanical strength towards wound healing application. *Journal of Materials Chemistry B*, 2018, 26, 7066-7075.
2. Ruut Kummala, **Wenyang Xu**, Chunlin Xu, Martti Toivakka. Stiffness and swelling characteristics of nanocellulose films in cell culture media. *Cellulose*, 2018, 25(9), 4969-4978.
3. Saina Kishani, Francisco Vilaplana, **Wenyang Xu**, Chunlin Xu, Lars Wågberg. On the solubility of softwood hemicelluloses. *Biomacromolecules*, 2018, 19(4), 1245-1255.
4. Jinze Dou, **Wenyang Xu**, Jari J. Koivisto, Justin K. Mobley, Dharshana Padmakshan, Martin Kögler, Chunlin Xu, Stefan Willför, John Ralph, Tapani Vuorinen. Characteristics of hot water extracts from the bark of cultivated willow (Salix sp.). *ACS Sustainable Chemistry & Engineering*, 2018, 6(4), 5566-5573.
5. Yongchao Zhang, Menghua Qin, **Wenyang Xu**, Yingjuan Fu, Zhaojiang Wang, Zongquan Li, Stefan Willför, Chunlin Xu, Qingxi Hou. Structural changes of bamboo lignin during a combined fractionation process of autohydrolysis followed by formic acid rapid-delignification under pressure. *Industrial Crops & Products*, 2018, 115, 194-201.
6. **Wenyang Xu**, Henrik Grénman, Dennis Kronlund, Jun Liu, Bin Li, Jouko Peltonen, Anna Sundberg, Stefan Willför, Chunlin Xu. Mild oxalic acid-catalyzed hydrolysis as a novel approach to prepare cellulose nanocrystals. *ChemNanoMat*, 2017, 3(2), 109-119**.**
7. Rose-Marie Latonen, Anni Määttänen, Petri Ihalainen, **Wenyang Xu**, Markus Pesonen, Maristiina Nurmi, and Chunlin Xu. Conducting Ink Based on Cellulose Nanocrystals and Polyaniline for Flexographical Printing. *Journal of Materials Chemistry C*, 2017, 5, 12172-12181.
8. Yongchao Zhang, Qingxi Hou, **Wenyang Xu**, Menghua Qin, Yingjuan Fu, Zhaojiang Wang, Stefan Willför, Chunlin Xu. Revealing the structure of bamboo lignin obtained by formic acid delignification at different pressure levels. *Industrial Crops and Products*, 2017, 108(1), 864-871.
9. Jun Liu, Gary Chinga-Carrasco, Fang Cheng, **Wenyang Xu**, Stefan Willför, Kristin Syverud, Chunlin Xu. Hemicellulose-reinforced nanocellulose hydrogels for wound healing application. *Cellulose*, 2016, 23(5), 3129-3143.
10. Bin Li, **Wenyang Xu**, Dennis Kronlund, Anni Määttänen, Jun Liu, Jan-Henrik Smått, Jouko Peltonen, Stefan Willför, Xindong Mu, Chunlin Xu. Cellulose nanocrystals prepared *via* formic acid hydrolysis followed by TEMPO-mediated oxidation. *Carbohydrate Polymers*, 2015, 133, 605-612.
11. **Wenyang Xu**, Andrey Pranovich, Xiaoju Wang, Stefan Willför, Chunlin Xu. 15th European Workshop on Lignocellulosics and Pulp (EWLP), Aveiro, Portual, June 26th-29th, 2018. (Oral presentation by Wenyang Xu with **Best Oral Award**)
12. Binbin Zhang, Chunlin Xu, Jun Liu, Xiaoju Wang, **Wenyang Xu**, Fang Cheng, Paul Molino, Gordon Wallace, Stefan Willför. 3D Printing of Wood-based Nanocellulose Scaffolds for Biomedical Applications. International Conference on

Nanoscience and Nanotechnology (ICONN), Wollongong, Australia, January 29th -February 2nd, 2018. (Oral presentation by Binbin Zhang)

13. Chunlin Xu, **Wenyang Xu**, Andrey Pranovich, Stefan Willför. Tailoring wood-based functional materials by 3D printing – value-added approaches. Syysseminaari ja XI Johan Gullichsen-Kollokvio, Helsinki, Finland, November 8th, 2017. (Poster presentation by Chunlin Xu)
14. **Wenyang Xu**, Bin Li, Stefan Willför, Anna Sundberg, Chunlin Xu. Novel approaches to prepare cellulose nanocrystals by mild carboxylic acid-catalyzed hydrolysis. International Symposium of Nanocellulosic Materials, Hangzhou, May 20th-22nd, 2017. (Oral presentation by Bin Li)
15. Erica Sjöholm, Heidi Öblom, **Wenyang Xu**, Chunlin Xu, Stefan Willför, Niklas Sandler, Maren Preis. Application of a three-dimensional bioprinter for the deposition of an active substance onto wound healings. 2nd European Conference on Pharmaceutics, Krakow, Poland, April 3rd–4th, 2017. (Poster presentation by Erica Sjöholm)
16. **Wenyang Xu**, Henrik Grénman, Jun Liu, Anna Sundberg, Stefan Willför, Chunlin Xu. Mild oxalic acid-catalyzed hydrolysis as a novel approach to prepare cellulose nanocrystals, Nordic Wood Biorefinery Conference, Stockholm, Sweden, April 27th-30th, 2017. (Oral presentation by Wenyang Xu)
17. **Wenyang Xu**, Henrik Grénman, Jun Liu, Stefan Willför, Anna Sundberg, Chunlin Xu. Preparation of cellulose nanocrystals by mild oxalic acid-catalysed hydrolysis. Younger Researcher Seminar of The Marcus Wallenberg Prize, Stockholm, Sweden, October 10th-13rd, 2016. (Poster Presentation by Wenyang Xu)
18. **Wenyang Xu**, Jun Liu, Stefan Willför, Chunlin Xu. Preparation of cellulose nanocrystals via formic acid hydrolysis followed by TEMPO-mediated oxidation. Final PolyRefNorth Seminar, Norway, November 26th-27th, 2015. (Poster Presentation by Wenyang Xu)

Abstract

Three-dimensional (3D) printing has shown promising potential in fabrication of complex tissue with a structural control from micro- to macro-scale, meeting the requirements of tissue engineering. Wood-derived biopolymers as a category of biomaterials have attracted great attention as the feedstock materials in 3D printing owing to their abundant availability, biocompatibility, and *in vitro* biodegradability. However, the key issues are to tailor wood-derived biopolymers to 3D printable ink formulations and maintaining shape fidelity. The work of this thesis is dedicated to developing different types of ink formulations to be used in biomedical applications concerning the utilization of wood-derived biopolymers in a highly valuable and efficient way.

Firstly, the *O*-acetyl-galactoglucomannan (GGM), a side-stream biopolymer from Norway spruce, was investigated for filament preparation with poly-lactic acid (PLA) in its native and bulk form. A solvent blending approach was established to blend GGM and PLA together for further PLA/GGM filament preparation. As much as 20% of the PLA could be replaced by GGM without decreasing the mechanical properties of the filament. 3D scaffolds were successfully printed from the polymer blends by fused deposition modeling 3D printing. The biocompatible and biodegradable feature of wood-derived hemicelluloses would potentially boost this new composite ink in various biomedical applications such as tissue engineering and controlled drug release.

Cellulose nanofibrils (CNFs), a product of nanomaterials from cellulose, have been studied in formulating hydrogel inks owing to their intrinsic properties of the shear thinning behavior, structural similarity to extracellular matrix, and biocompatibility. The formulation of TEMPO-oxidized CNFs with gelatin methacrylate (GelMA) into low-concentration bioinks facilitated the cross-linking ability of GelMA ($\leq$ 1 w/v %), and further enhanced the shape fidelity of the printed scaffolds. 3D printable low-concentration inks showed promising potential in tissue engineering due to the relative loose polymer network that can encourage cell-cell interaction, migration, and more efficient metabolism.

GGM as a polysaccharide with abundant hydroxyl groups was chemically modified to be used as the cross-linker for CNF-based inks. Two derivatization approaches were established. In one approach, TEMPO-mediated oxidation was applied to introduce carboxylic groups, which were further reacted with tyramine to obtain tyramine-conjugated GGM. In the other approach, GGM methacrylate was synthesized in a facile and green process under aqueous condition. Both tyramine-conjugated GGM (GGMTA) and GGM methacrylate (GGMMA) were separately studied to successfully form gel by enzymatic and UV-aided cross-linking, respectively.

Furthermore, surface-engineered biomimetic inks were formulated with GGMMA and CNFs thanks to the intrinsic affinity of GGM to cellulose fiber

surfaces mimicking the plant cell wall. The formulated homogeneous inks facilitated the high-resolution printing of complex scaffolds and geometries. More importantly, the stiffness of the resulted hydrogels was tunable in a wide spectrum ranging from 2.5 to 22.5 kPa by controlling the degree of substitution of methacrylate and compositional ratio of CNFs and GGMMA. As a new family of 3D printing feedstock materials, the CNF/GGMMA inks will broaden the map of bioinks, which potentially meet the requirements for a variety of *in vitro* cell-matrix and cell-cell interaction studies in the context of tissue engineering, *e.g.* cancer cell research, and high-throughput drug screening.

Lastly, the biocompatibility of the CNF-based bioinks was proven with incubating 3T3 fibroblast cells. The mechanical properties and topography of the printed scaffolds with CNF/GelMA inks could manipulate the cell attachment and promote cell proliferation. The developed low-concentration ink formulations with a facile yet effective approach to fabricate scaffolds show a great deal of potential in bioprinting for wound healing and soft tissue regeneration.

Keywords

3D printing, *O*-acetyl-galactoglucomannan (GGM), biocomposite, biomedical applications, cellulose nanofibrils (CNFs), direct ink writing (DIW), enzymatic cross-linking, fused deposition modeling (FDM), gelatin methacrylate (GelMA), GGM methacrylate (GGMMA), low-concentration ink, poly-lactic acid (PLA), tyramine-conjugated GGM (GGMTA), UV cross-linking, wood-derived biopolymer, wound healing

Svensk sammanfattning

Tredimensionell (3D) printing har visat en lovande potential vid tillverkning av komplex vävnad med strukturell kontroll från mikro- till makroskala, som uppfyller kraven för vävnadsteknik. Användning av träbaserade biopolymerer i 3D-printning har väckt stort intresse tack vare deras rikliga tillgänglighet, biokompatibilitet och biologiska nedbrytbarhet in vitro. Väsentligt är emellertid att kunna skräddarsy träbaserade biopolymerer till bläck som kan användas i 3D-printning samt att de strukturer som printats bibehåller sin fysiska form. Syftet med denna avhandling är inriktat på att utveckla olika typer av bläck som kan användas i biomedicinska tillämpningar kombinerat med att utnyttja träbaserade biopolymerer på ett värdefullt och effektivt sätt.

Först undersöktes O-acetyl-galaktoglukomannan (GGM), en biopolymer som kan isoleras från sidoströmmar vid användningen av finsk gran. Den naturligt förekommande formen av GGM blandades med polymjölksyra (PLA) och filament tillverkades. Så mycket som 20 % PLA kunde ersättas med GGM utan att filamentets mekaniska egenskaper försämrades. 3D-strukturer printades framgångsrikt av dessa filament genom 3D-printning med material-extruderingsteknik (fused deposition modeling, FDM). De biokompatibla och biologiskt nedbrytbara egenskaperna hos träbaserade hemicellulosor skulle kunna öka tillämpningen av detta nya kompositbläck i olika biomedicinska applikationer, såsom vävnadsteknik och kontrollerad frisättning av läkemedel.

Cellulosa nanofibriller (CNF), ett nanomaterial från cellulosa, studerades vid formulering av hydrogeler för 3D-printning (s.k. biobläck, eller enbart bläck) på grund av deras egenskaper som skjuvningsförtunning, strukturell likhet med den extracellulära matrisen och biokompatibilitet. Formuleringen av TEMPO-oxiderad-CNF med gelatinmetakrylat (GelMA) i bläck med låg koncentration underlättade tvärbindningsförmågan hos GelMA och förbättrade ytterligare formfastheten hos de printade stödstrukturerna. 3D-printbara lågkoncentrationsbläck visade lovande potential för vävnadsteknik tack vare det relativt lösa polymernätverket som kan främja cellinteraktion, cellmigration och effektivare ämnesomsättning.

GGM, en polysackarid rik på hydroxylgrupper, modifierades kemiskt och användes som tvärbindare för CNF-baserade bläck. Två derivatiserings-metoder etablerades. TEMPO-medierad oxidering användes för att införa karboxylgrupper, vilka vidare reagerade med tyramin för att erhålla tyraminkonjugerad GGM (GGMTA). I den andra metoden syntetiserades GGM-metakrylat (GGMMA) i en enkel och grön process i vattenmiljö. Framgångsrika tester visade att både GGMTA och GGMMA bildade tvärbundna gel efter enzym- eller UV-behandling.

Vidare formulerades ytmodifierade, biomimetiska bläck med GGMMA och CNF tack vare affiniteten av GGM till cellulosafiberytor som efterliknar

strukturen i en växtcellvägg. De formulerade homogena bläcktyperna underlättade högupplösningsprinting av komplexa stödstrukturer och geometrier. Ännu viktigare var att styvheten hos de resulterande hydrogelerna kunde kontrolleras i ett brett spektrum, från 2,5 till 22,5 kPa, genom att variera graden av substitution av metakrylat och förhållandet mellan CNF och GGMMA. Som en ny familj av 3D-printningsmaterial, kommer CNF/GGMMA-bläcken att öka utbudet av biobläck som potentiellt uppfyller kraven för olika in vitro-cellmatris och cellinteraktionsstudier i samband med vävnadsteknik, t.ex. cancercellsforskning och läkemedelsscreening.

Slutligen visades biokompatibiliteten hos de CNF-baserade biobläcken med inkubation av 3T3 fibroblastceller. De mekaniska egenskaperna och topografin hos de printade stödstrukturerna med CNF/GelMA-bläck kunde manipulera hur cellerna fäste sig och främja cellspridningen. De utvecklade lågkoncentrationsbläcken, som kan användas på ett enkelt och effektivt sätt för att tillverka stödstrukturer, har en stor potential vid bioprinting för sårläkning och mjukvävnadsregenerering.

List of important abbreviations

3D	Three-dimensional
AFM	Atomic force microscopy
BNC	Bacterial nanocellulose
CAD	Computer-aided design
CNCs	Cellulose nanocrystals
CNFs	Cellulose nanofibrils
CNW	Cellulose nanowhiskers
DCM	Dichloromethane
DIW	Direct ink writing
DMF	Dimethylformamide
DMSO	Dimethyl sulfoxide
DS	Degree of substitution
DSC	Differential scanning calorimetry
ECM	Extracellular matrix
FDM	Fused deposition modeling
G'	Storage modulus
GC	Gas chromatography
GelMA	Gelatin methacrylate
GGM	Galactoglucomannan
GGMMA	GGM methacrylate
GGMTA	Tyramine-conjugated GGM
HME	Hot melt extrusion
HPSEC	High performance size exclusion chromatography
HRP	Horseradish peroxidase
MA	Methacrylate group
Mn	Average number molecular weight
Mw	Average weight molecular weight
NCC	Nanocrystalline cellulose
NMR	Nuclear magnetic resonance
PCL	Poly-caprolactone
PEI	Polyethylene imine
PLA	Poly-lactic acid
QCM-D	Quartz crystal microbalance with dissipation monitoring
SEM	Scanning electron microscopy
TA	Tyramine
TEM	Transmission electron microscopy
TEMPO	2,2,6,6-tetramethylpiperidine-1-oxyl radical
Tg	Glass transition temperature
TGA	Thermal gravimetric analysis
Tm	Melting temperature

1. Introduction

1.1 Tissue engineering and extracellular matrix scaffolds

Extracellular matrix (ECM) is secreted by cells in the form of 3D networks. ECM biologically provides structural and biochemical support for the surrounding cells. [1, 2] The animal ECM includes a basement membrane and an interstitial matrix in the form of hydrogel from polysaccharides and fibrous proteins such as collagen, elastin, and laminins (**Figure 1.1**). The secretion of a complex and specific ECM is done by the synthesis of matrix macromolecules with different cell types. [3] These specific ECMs modulate tissue dynamics *via* the bioactivity of binding and releasing bioactive molecules making the communications and signaling between cells and the surrounding ECM. [4] ECM has been verified for regulating cell fate by its chemical and physical properties such as surface chemistry, viscoelasticity, porosity, diffusivity, and mechanical properties both in surface and in bulk. [5]

Tissue engineering is the tissue regeneration process combining cells from patients as well as a highly porous artificial scaffold with nutrients and growth factors mimicking an *in vivo* environment that modulates cell behaviors in three dimensions. [6] Thus, the artificial scaffold in the tissue engineering process is much about mimicking the ECM. [7] The artificial scaffold should support the cells as a platform and guide them to start secreting their own ECM. The designed scaffold should meet several requirements such as supporting cell adhesion and migration, enabling diffusion of growth factors and metabolic wastes, and having the targeted mechanical response to cells. [8] Thus, the artificial ECM should be a particular biological microenvironment to obtain cell and tissue specificity. Moreover, the artificial scaffold should have efficiently and adequately connective pores to allow cell growth through the structure for further obtaining a tissue. [9] Ideally, the scaffold material in terms of biomaterial should be degradable without hindering the formation of new tissue.

Wounds are considered as ‘the silent epidemic’. [10] Wounds are generally caused by surgical intervention, injury, burn, as well as other extrinsic factors and underlying conditions such as pressure, shear, diabetes, and vascular disease. [11] According to the causes, wounds are defined into acute wounds including surgical wounds and burns, and chronic wounds such as diabetic foot ulcers. [10] Chronic wounds are also defined as ‘hard-to-heal’ wounds, which lead a huge and preventable burden to patients with suffering pain, depression, social isolation, and extended hospital stay. Annually, the population prevalence of wounds is three to four persons per one thousand population with an incidence of 4 million individuals cross Europe. [12] The global volume of wound managements has severe healthcare implications, and leads to about half of the world's annual expenses regarding the stay in hospital, the use of professionals’ time, the choice of materials and treatments in the healthcare

sector. [13] For example, the cost of managing diabetic foot ulcers is estimated to be four to six billon euro per year. [14] Thus, tissue engineering is emerging for better medication solutions and more efficient treatments especially for chronic wounds, which are particularly common among the elder population. In conventional tissue engineering, treatments mostly rely on harvesting autologous, allogenic, or xenogeneic tissues, encountering various serious problems, such as the lack of donor, the undesirable responses of immune system, and the risk of pathogen transmission. [15, 16] To address these issues, the biopolymer-based scaffolds can be potentially manufactured to incorporate the cells and biomolecules and act as analogues to the natural ECM in tissues.

The biomaterials for mimicking ECM could be defined into three categories including ceramics, synthetic polymers, and natural polymers. [17] Ceramic scaffolds such as hydroxyapatite, tri-calcium phosphate, and bioactive glasses with typical high mechanical stiffness are mostly used in bone regeneration, dental, and orthopedic surgeries. However, the brittleness and difficulty of being shaped have limited their application in scaffold fabrication. Synthetic polymers such as poly-lactic acid (PLA), polystyrene, and poly-caprolactone (PCL) have been used in the attempt to fabricate biological scaffolds due to the ease of being fabricated with tailored architectures and degradation characteristics. However, the hydrophobic nature of the synthetic bioplastics might inhibit their biocompatibility. [18] The natural biomaterials such as collagen and its derivatives, alginate-, and chitosan-derived biomacromolecules, as well as decellularized extracellular matrix (dECM) attracted great attention as the ECM-mimicking precursors owing to their inherent biocompatibility, bioactivity, and biodegradability. Collagen is one major component of animal ECM. The derivatives of collagen like gelatin and gelatin methacrylate (GelMA) could also be used for making artificial scaffolds under different cross-linking strategies, because it is the most abundant protein containing cell-adhesion domain sequences. [19-21] However, collagen has the risks of being recognized as foreign by the immune system. [22] Other natural biopolymers such as chitosan and alginate have also been widely studied as materials mimicking ECM. [23, 24] Recently, cellulose has shown promising potential in tissue engineering due to the properties of hydrophilicity, biocompatibility, easily controlled surface chemistry, fibril-like, possible gelation, and capability to form porous structures. [25, 26]

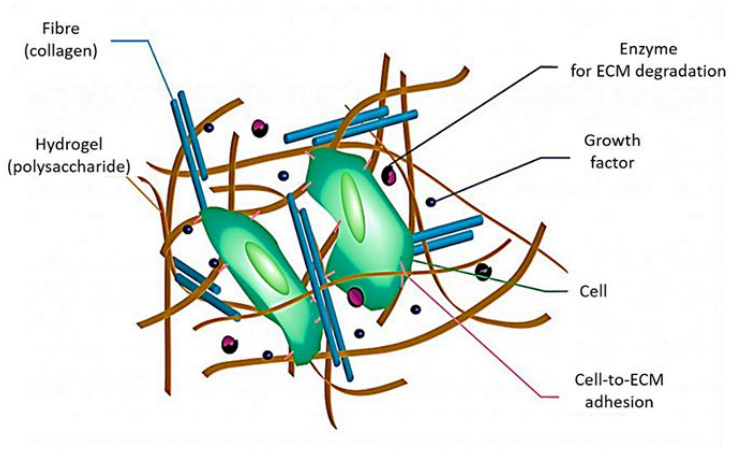

Figure 1.1. *Schematic image of the ECM including the distribution of cells, polysaccharides, fibrous proteins, matrix-degrading enzymes, and growth factor. Image was adapted from website. [27]*

1.2 Wood as a new material resource

Trees offer us sustainable and renewable materials concerning the integration of water, sun (energy), air, and soil (ions) in nature during their growth. Wood from trees could be utilized as a composite material or polymer raw materials in different scales from solid wood to monomer sugars. The processing method determines the forms and types of wood-derived materials, which could be utilized in a wide range. So far, wood as a material resource influences our daily life in different forms of construction, furniture, paper, food additives, and medical supplies. [28] The utilization of wood-derived advanced materials could increasingly benefit sustainable developments in the areas of biotechnology, bioengineering, and bioeconomy in novel and versatile ways. [29-31]

As a tissue, wood presents a highly hierarchical structure, as schematically illustrated in **Figure 1.2**. Morphologically, the cell wall of wood tissues is composed of different cell wall layers surrounded by amorphous and intercellular substances giving the trees strength and other physical properties. [32] The cell wall in wood tissues is divided into the middle lamella (ML), primary wall (P), and the secondary walls (S). In the primary cell wall, the microfibrils (diameter of 10-40 μm and up to a few mm in length) are loosely packed and randomly arranged. The secondary walls are composed of the outermost layer S1, the middle layer S2, and innermost layer S3. The microfibrils of the three secondary walls are directed and oriented with different angles. [33] The microfibrils in both primary and secondary cell walls consist of aggregated fibrillary bundles with a lateral dimension of 10-30 nm and over one μm in length. These fibrillary aggregates are composed of elementary fibrils around 40 cellulose chains and diameter ranging from 1.5 to 3.5 nm. [34]

Moreover, in the secondary cell walls, microfibrils are integrated with hemicelluloses and lignin participating the formation of wood tissue composite.

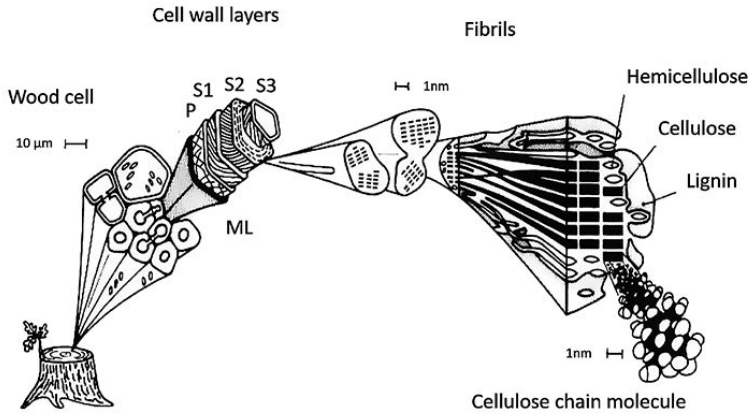

Figure 1.2. *The hierarchy of the wood tissue cell wall. Adapted with permission from Copyright (1990) American Chemical Society. [35]*

Chemically, the main compositions of the wood is cellulose (45-50%), hemicelluloses (20-25%), lignin (20-30%), and other extractives. [36] Cellulose is a linear homopolymer consisting of D-glucopyranose-units linked together *via* β-1,4 glycosidic bonds. [34, 37] The sugar unit is with the glucosyl ring in $^4C_1$ chair configuration and one primary and two secondary hydroxyl groups. The inter- and intra-molecular hydrogen bond network is formed between and within the cellulose chains by these free hydroxyl *groups*, which contribute to the formation of highly ordered crystalline regions. [38]

Hemicelluloses are mainly heterogeneous polysaccharides. However, they have the same function of supporting material in cell walls as cellulose. The content and composition of hemicelluloses vary among species and among different parts of the tree. In comparison to cellulose, hemicelluloses can be branched, partially water-soluble polymers, with lower degree of polymerization (DP) ranging from less than 100 to about 200 sugar units. [39] The main chain of hemicelluloses usually consists of two or more sugar units. In softwoods, the most abundant hemicelluloses are *O*-acetyl-galactoglucomannans (20-25%), referred to as GGM. Moreover, softwoods also contain arabinoglucurunoxylans (5-10%), xyloglucans, and other glucans. [40] In hardwoods, xylans, especially *O*-acetyl-4-O-methylglucuronoxylans, are the major hemicellulose type, representing about 80-90% of the hardwood hemicelluloses. [41, 42]

Lignin, a mixture of amorphous aromatic polymer, is a significant organic substance in lignocellulosic biomass. The build-unit of lignin is the phenylpropane unit including *p*-coumaryl alcohol, coniferyl alcohol, and sinapyl alcohol. In wood tissues, lignin is considered to have the functions of

making the cell wall stiff, gluing cells together, and increasing resistance towards biodegradation. [43, 44]

Extractives comprise many different substances, mainly with low molar mass. Broadly, extractives can be divided into two groups: lipophilic and hydrophilic extractives. Extractives mainly maintain the biological function of the tree and provide protection from microorganisms. [45]

1.3 Nanocellulose

Nanocellulose, the cellulose with at least one dimension in nanoscale, has received an immense attention due to its outstanding and fascinating structural and chemical properties. Based on the differences in the preparation methods, morphology, and functions, nanocelluloses have been classified into three categories: bacterial nanocellulose (BNC), cellulose nanofibrils (CNFs), and cellulose nanocrystals (CNCs). [46] BNC are mainly be prepared *via* bottom-up construction in a culture medium with certain types of microorganisms through oxidative fermentation. [47] On the contrary, both CNFs and CNCs are prepared using top-down methods starting from biomass. For CNFs, some of the interfibrillated hydrogen bonds in biomass are broken by mechanical disintegration to form fibrils with micrometer size in length and nanometer size in width. Thus, both the crystalline and non-crystalline regions are present in CNFs. The preparation of CNCs can be achieved by the removal of non-crystalline regions in the fibers mostly through acid hydrolysis. A proposed co-existence of crystalline and non-crystalline regions of cellulose fibers is shown in **Figure 1.3**.

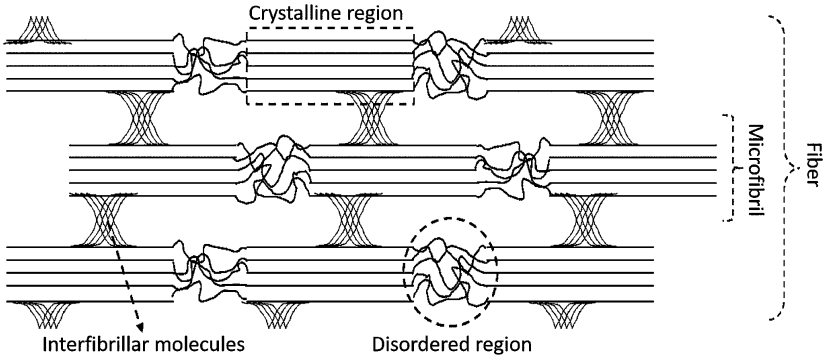

Figure 1.3. *Illustration of cellulose fibers with both crystalline and non-crystalline regions. Image was adapted with permission from the open publisher, IntechOpen. [48]*

1.3.1 Bacterial nanocellulose (BNC)

Bacterial nanocellulose was first reported in 1866 after the observation of the growth of unbranched pellicle with a similar structure as the plant cellulose. [49] In 1950s, the synthesis of BNC occurred by the study using *Acetobacter xylinm* as the model bacterium with the culture medium containing glucose and oxygen. [50] Since then, various bacterial strains such as *Acetobacer*, *Achromobacter*, *Aerobacter*, *Gluconacetabacter xylinus*, *Lactobacillus mali*, *Pseudomonas*, *Rhozobium*, *Sarcina* have been used for the preparation of BNC investigating the production efficiency, raw carbon source, and the function of additives in culture media. Among them, *Gluconacetabacter xylinus* is considered as the most efficient one. [47] During culturing, the medium with microorganisms should be respectively oxygenated at a pH below 5 and optimal temperature (25-30 °C). [51] Fibrils are synthesized and secreted as exopolysaccharide to the aqueous medium. Further, the secreted fibrils are combined with the ribbons generating a 3D hydrogel network. **Figure 1.4** shows the preparation of BNC by *Gluconacetobacter* bacteria and SEM images of BNC samples.

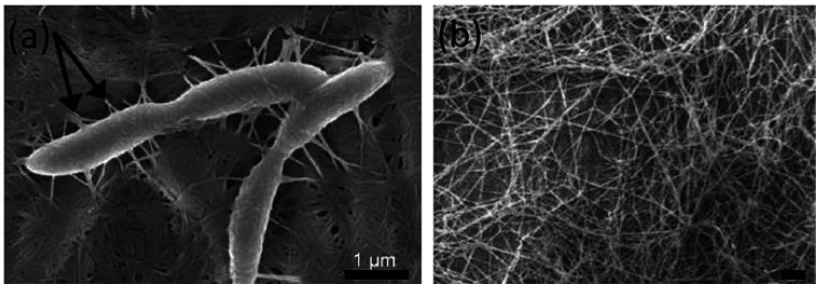

Figure 1.4. *(a) The BNC preparation with* Gluconacetobacter bacteria, *and (b) SEM image of a bacterial nanocellulose sample presenting a coherent 3D network. The scale bar presenting one µm. Images were adapted with permission from open access Sciendo and Nova Science Publishers Inc. [51, 52]*

BNC possesses intriguing properties such as ultra-fine dimensions with 2-4 nm in diameter, high degree of polymerization (up to 10,000), high crystallinity (> 85%), and high mechanical strength with the Young's modulus of individual BNC over 60 GPa. [53, 54] Physically, BNC has high water absorption capacity to form 3D networks. [55] Based on those, BNC has been successfully studied in biomedical applications such as dressing material and artificial skin for wound healing, blood vessel, vascular implants, and cartilage implants. [55-58] Moreover, BNC showed promising potential in the applications, *e.g.* as emulsion stabilizer for cosmetics, as dietary fiber in food industries, and as reinforcement agents in fiber-based biocomposites. [59-61] However, the yield and productivity of BNC regarding cost-effectiveness of culture medium require further efforts and improvements. [62]

1.3.2 Cellulose nanofibrils (CNFs)

Cellulose nanofibrils are mainly manufactured by mechanical defibrillation disintegrating the large fiber bundles to small fibrils. CNFs were first reported by this method in the beginning of the 1980s. [63, 64] Still now, the preparation of CNFs is mainly proceeded by the methods of mechanical disintegration such as grinding, cryo-crushing, high-pressure fluidizers, and high-pressure homogenizer. However, the high energy consumption with over 25000 kWh/ton became one of the key issues in preparation of CNFs. [46] To reduce the intensive energy consumption, enzymatic and/or chemical pretreatment steps have been developed and applied prior to the defibrillation process. [65] In the meantime, the surface chemistry of the prepared CNFs can be manipulated differently through different chemical pretreatments. For example, the pretreatment with 2,2,6,6-tetramethylpipelidine-1-oxyl (TEMPO) oxidation can yield an increasing amount of carboxylic groups and aldehyde groups on the surface of the CNFs. [66] Another commonly used method is carboxymethylation to turn the surface of CNFs more anionic. [67] The proposed mechanism of TEMPO-mediated oxidation is shown in **Figure 1.5**. To prepare cationic CNFs, the fibers can be reacted with glycidyltrimethylammonium chloride, [68] N-(2-3-epoxypropyl) trimethylammonium chloride (EPTMAC) or chlorocholine chloride,[69] or absorbed with cationic polyelectrolytes like polyethylenimine (PEI), polydiallyldimethylammonium chloride (PDADMAC) or polyallylamine hydrochloride (PAH). [67] Nevertheless, the preparation of CNFs could be proceeded utilizing versatile sources such as wood, sawdust, sugar beet, hemp, and flex. [70]

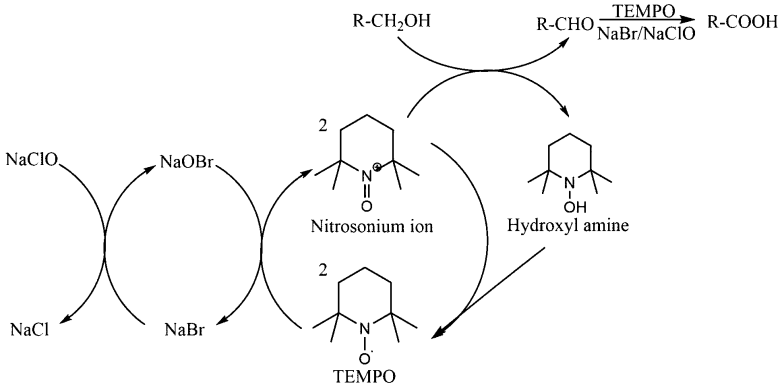

Figure 1.5. *Proposed mechanism for TEMPO-mediated oxidation of CNF. Image was adapted with permission from Copyright (2010) ELSEVIER. [71]*

After mechanical defibrillation, the obtained CNFs in morphology is known for the 'spaghetti-like' fibrils with a diameter of 5-60 nm and a length of several hundred nanometers to a few micrometers showing high aspect ratio between 100-1000, flexibility, excellent mechanical properties, good thermal-stability, and non-cytotoxicity. [46, 72] More importantly, the rheology of CNF hydrogel

exhibits a typical shear-thinning and thixotropic property due to the abundant hydrogen bonding and self-entanglement. [73] An image of TEMPO-mediated CNFs and its morphological image by TEM are shown in **Figure 1.6**.

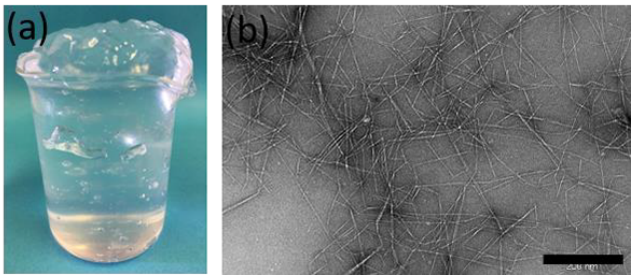

Figure 1.6. *(a) Image of CNFs made from TEMPO-mediated oxidation, and (b) TEM image of TEMPO-mediated CNFs with diameter less than 20 nm and length less than 1000 nm. Scale bar presenting 200 nm.*

In the past decades, CNFs have been investigated as a versatile material in the areas of electronics, cosmetics, pharmaceutics, and biomedicine. [28] Recently, CNF has gained tremendous attention to be used as a biomaterial platform in the field of biomedical applications due to its structural mimicry of ECM scaffolds. [25, 26] CNFs or CNF-based composites have been demonstrated as potential platform materials such as in wound healing application, for culturing human pluripotent stem cells, in cartilage regeneration. [74-77] So far, there are only a few commercial CNF-based biomaterial products in the market by UPM-Kymmene Oyj (Finland) with Growdex®, CELLINK AB (Sweden), and Borregaard (Norway) with EXILVA in the presence of microfibrillar cellulose.

1.3.3 Cellulose nanocrystals (CNCs)

Cellulose nanocrystals known as cellulose nanowhiskers (CNW) or nanocrystalline cellulose (NCC) were first reported in the 1950s and prepared by controlled sulfuric acid-catalyzed hydrolysis to remove the non-crystalline regions in the cellulose fibers. [78, 79] Acid hydrolysis with mineral acids is the most commonly used method to prepare CNCs. Instead of using mineral acids such as hydrochloric acid and nitric acid, acid hydrolysis with 64 wt.% sulfuric acid is the most conventional and efficient way to prepare CNCs. [80-82] However, certain issues such as harsh corrosion of equipment, large water consumption, severe environmental pollution, and low yield rate still need to be addressed considering the use of strong acids. To achieve a higher CNC yield and recycle the used acids, acid hydrolysis in less harsh condition employing solid acids and organic acids have been investigated. Recently, several studies utilizing phosphotungstic acid, formic acid, and oxalic acid established a sustainable route for the preparation of CNCs. [83-86] CNCs can also be prepared with TEMPO-mediated oxidation under both alkaline (pH range of 10-11.4) and acid-neutral conditions (the pH range of 3.5-6.8) [87] or enzymatic

hydrolysis combined with mechanical defibrillation. [88-90] With the mentioned methods, different functional groups can be introduced on the surface of CNCs. As a result, CNCs prepared with sulfuric acid can show a negatively charged surface with the introduction of sulfate groups ($-SO_3^{2-}$). CNCs with carboxylic groups ($-COO^-$) could be obtained by oxalic acid hydrolysis and TEMPO-mediated oxidation. Similarly to CNFs, the raw materials for the preparation of CNCs are in a wide range such as wood fibers, tunicate, bamboo, wheat straw, and tobacco stalk. [91-97]

CNCs prepared with different methods are shown in **Figure 1.7**. The resulting CNCs are rigid rod-like materials with a diameter of 3-50 nm and length of a few hundreds of nanometers. [98] Nevertheless, the morphology of the prepared CNCs can be manipulated by tuning the hydrolysis time, reaction temperature, and acid concentration. [99] Generally, the CNCs present an aspect ratio in the range of 20-50, excellent elastic modulus (~150 GPa), and high surface area (up to 419 m^2/g). [98, 100, 101] Uniquely, CNCs show intense macroscopic birefringence due to the chiral nematic structures. [102-104] CNCs as a versatile material have been proposed for a wide range of applications such as composite reinforcements, green catalysis, flocculants, stabilizer for nanoparticles, biosensing and bioimaging, antimicrobial materials, and in certain biomedical applications. [105-111]

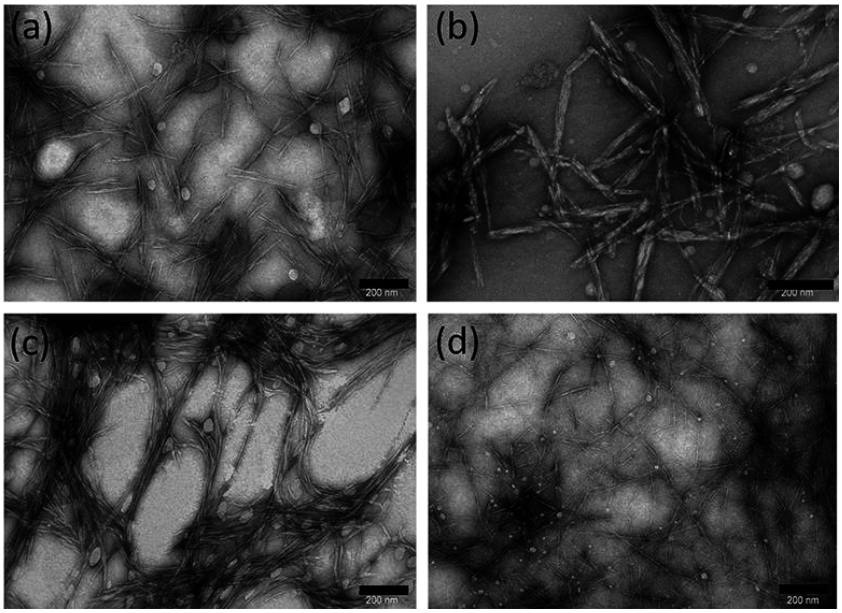

Figure 1.7. *TEM images of CNCs prepared from H_2SO_4 (a), oxalic acid (b), formic acid (c), and TEMPO-mediated oxidation (d), Scale bar presenting 200 nm.*

1.4 Hemicelluloses

Hemicelluloses accounting for average up to 50% of the biomass of annual and perennial plants are considered as the second most abundant polysaccharides in nature. [112] Hemicelluloses are found with lignin as a 'glue' firmly bonded with cellulose microfibrils in plant cell walls. The majority of hemicelluloses are xylans in hardwoods and glucomannans in softwoods. Nevertheless, other types of hemicelluloses such as arabinans, galactans, and glucans also exist. [113] Hemicelluloses are a group of hetero-polysaccharides containing either pentose or hexose with abundant free hydroxyl groups. These active hydroxyl groups are readily available for chemical modifications such as esterification, etherification, (regioselective) oxidation, or graft polymerization. [114-116] Due to the intrinsic properties with non-toxicity, biodegradability, and biocompatibility of hemicelluloses, the native and modified hemicelluloses have been of great interest with a wide spectrum of applications in different areas such as waste water treatment, food industry, cosmetics, pharmacy and medicine, *etc*. [112, 117] In the recent years, hemicelluloses have attracted increasing interests in the field of biomedical applications. For example, native hemicelluloses were proposed to be used with CNF hydrogel for wound healing application. [75] Several hemicellulose-based hydrogels were also prepared aiming at biomedical applications through different cross-linking strategies. [118-121]

O-acetyl galactoglucomannan (GGM)

O-acetyl galactoglucomannan is the most abundant hemicellulose type in softwood. GGM can be easily recovered from side-stream of spruce mechanical pulp processes, and also extracted from Norway spruce (*Picea abies*) wood chips by pressurized hot-water extraction. [122, 123] GGM consists of a linear backbone of randomly distributed (1→4)-linked-β-D-mannose and (1→4)-linked-β-D-glucose unites, with (1→6)-linked-α-D-galactose units as single side chains, [124] as shown in **Figure 1.8**. GGM is partially acetylated with *O*-acetyl groups located randomly at the C2 and C3 position of the mannose units in the main chain. Depending on the way of isolation and the purification methods, the molar mass of GGM can vary between 5-60 kDa. The sugar ratio of mannose:glucose:glactose in the GGM polymer chain is approximately 3.5-4.5:1:0.5-1.1. [125] Naturally acetylated GGM is soluble in water, dimethyl sulfoxide (DMSO), and dimethylformamide (DMF), and could be accessible and capable of being functionalized with different chemical reactions.

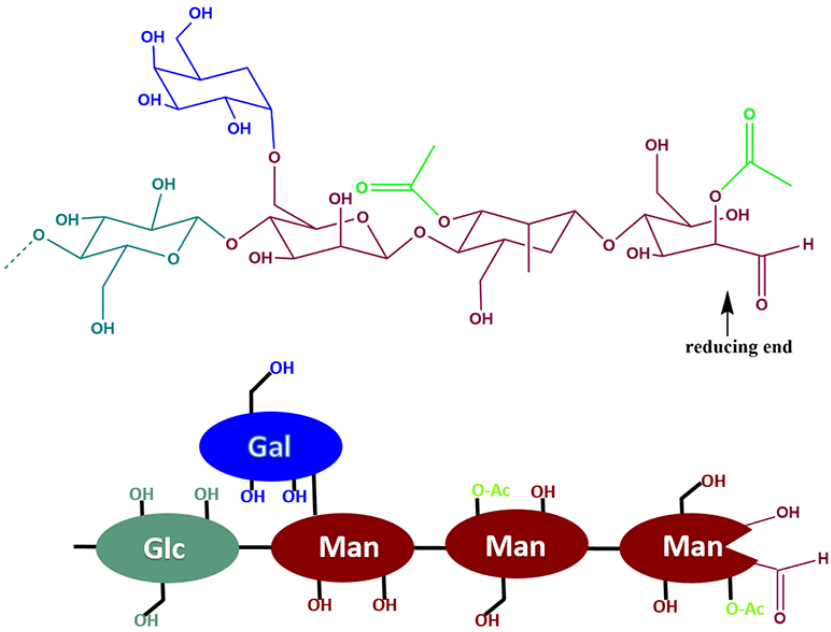

Figure 1.8. *Illustration of chemical structure of O-acetyl-galactoglucomannan with Glc for glucose, Gal for galactose, and Man for mannose.*

1.5 Three-dimensional printing and ink formulation

3D printing, as one type of additive manufacturing (AM) techniques, provides a bottom-up approach to rapidly fabricate complex object geometries layer-by-layer using slicing with computer-aided design (CAD). [126] As a simple model of 3D printing, a gantry-robot is fitted with the printing head moving in X- and Y-axis, and the printing platform moves in vertical Z-axis. The moving of either printing head up or printing platform down will facilitate the subsequent layer printing on the deposited layer in the defined layer thickness. With continuous layer-by-layer deposition, a quick transfer from ideas to real objects advances the possibility to produce, repair, and replace objects on-demand. The same objects could also be manufactured in a simplified methodology with the same printing technology and available materials wherever in the world, at whenever the time, and with whoever the specialists. [127] Thus, 3D printing offers the promise of manufacturing in a less-energy, less-waste, and low-cost supply chain. Generally, the 3D printing techniques are classified into sheet lamination, powder bed fusion, binder jetting, direct energy deposition, vat photo-polymerization and extrusion. [128, 129] With different 3D printing techniques, one can print plastics, wood, metals, ceramics, food and even living cells. In short, few basic requirements are needed regarding 3D printing: the digital design, the 3D printing technique, and the ink materials.

1.5.1 Extrusion-based 3D printing technology

The extrusion-based 3D printing techniques are to extrude and consequently solidify the inks after it emerges from the printer head. The objects are built up layer-by-layer until the whole object is completed. Within this type of techniques, there are basically two kinds: fused deposition modeling (FDM), and direct ink writing (DIW). The materials used in extrusion-based 3D printing techniques should be either possible to be molten or as an extrudable thick gel or slurry.

The FDM technique is considered as a simple and cost-effective approach, as illustrated by **Figure 1.9a**. FDM based on material molten flow-solidification utilizing filaments as the shape of feedstock materials. As a combined technique, hot melt extrusion (HME) is mostly required for the filament preparation. [130] The well-shaped filaments produced by the HME process pass through the feeding roller, heater, and nozzle, followed by the melt paste deposition on a printing platform. The whole geometry can be obtained after all the layers have been deposited. Currently, multiple extrusion heads can be applied in FDM for using different materials at the same time, which enables printing of more complex geometries. In order to build complex shaped parts, supporting materials apart from the building material are usually required. The supporting materials can support the overhanging structures during the printing process and help maintaining the structural integrity. The supporting parts can be removed by dissolving in an appropriate solvent or breaking without destroying the main structural body.

The DIW technique was first developed at the Freiburg Materials Research Centre in 2000 to create soft tissue scaffolds, as shown in **Figure 1.9b**. [131] The process can be done at room or elevated temperature but not involving thermoplastics as FDM. The inks must have an adequate rheological moduli, shear-thinning properties, and thixotropic behavior. [132, 133] Most of the time, the inks are stored in a syringe-like reservoir connected with the dispensing tips with different shape and size on the printer head. The displacement of the syringe piston by mechanical screw or air pressure causes the flow of the inks with further stress inside the dispensing tip. The obtained stress results in a decrease of ink viscosity to drive the ink flow, which is so-called yield-flow property. As the deposition of the ink occurs, the stress disappears. Then, the ink relaxes and forms the designed geometry resulting in the complete process of the 3D prototype.

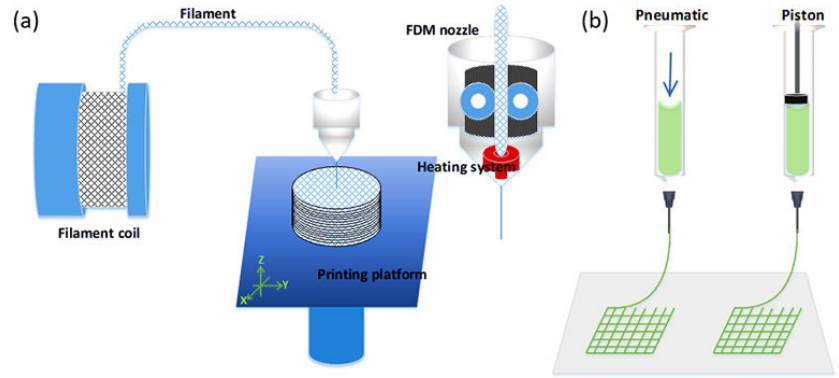

Figure 1.9. *Extrusion-based 3D printing techniques: (a) FDM 3D printing, and (b) DIW 3D printing with pneumatic- and piston-driven systems. Images were reproduced with permission from Copyright (2018) American Chemical Society. [134]*

1.5.2 Filaments

The most important selection criteria for FDM filaments are the heat transfer characteristics and the rheology behavior under molten state. Thermoplastics are a type of suitable materials for FDM 3D printing due to their glass transition temperature (Tg) and melting temperature (Tm). Thermoplastics such as PLA, PCL, ethylene-vinyl acetate (EVA), and acrylonitrile butadiene styrene (ABS) have been successfully applied as filament feedstock materials. [135-141] For example, PCL is well studied in biomedical applications with FDM 3D printing due to its low melting temperature around 60 °C. [142] PLA normally has the Tg in the range of 40-60 °C, and melting temperature around 150-170 °C. [143, 144] Furthermore, the materials must have high thermal-stability without severe degradation during filament manufacturing *via* HME processing and FDM printing, *i.e.* the temperature of thermal degradation must be below the setting temperature for the HME process and the FDM printing.

1.5.3 Hydrogels inks

Good printability can be achieved in DIW when hydrogels inks are prepared with different chemical and mechanical methods. In general, inks must be adequately formulated with such properties as: 1) easily flowing through dispensing tip with low resistance, 2) keeping the structure stably after emerging from the tip, and 3) having enough high mechanical properties to maintain the 3D structure. The key advantages of DIW inks are the material flexibility and possibility of being proceeded at room temperature. However, hydrogels with low stiffness will cause the issues of low resolution and collapse of the structure limiting the complexity of the shapes.

In order to increase the shape fidelity of the printed structure, different cross-linking strategies such as chemical, ionic, enzymatic, thermal or pH-dependent, and UV cross-linking are typically and easily applied during or after printing. [134, 145] Chemical cross-linking is the most direct way to fix the shape of the printed objects and requires extra cross-linking reagents and specific reaction conditions. Ionic cross-linking is a simple and effective way to cross-link the manufactured scaffolds. However, the cross-linking rapidly initiates on the skirt and surface of the complex scaffolds resulting in the formation of shell on the skirt and surface, and further inhibits the transfer of ions to the inner structure of the 3D constructs. Moreover, the 3D constructs cannot keep their shape well when the scaffolds are transferred into a cell culture medium, which usually is less ionic. Enzymatic cross-linking is a mild way to achieve shape fidelity. However, the gelation window takes even a few hours, limiting its applicability in biofabrication. UV- and thermal-induced cross-linking offers a very short gelation time window, which is required for *in situ* gelation during biofabrication.

Recently, natural materials such as alginate, chitosan, collagen, gelatin, gelatin methacrylate, and cellulose nanofibrils, in the form of hydrogel have shown promising potential as bioinks in the field of biomedical applications due to their biocompatibility and biodegradability. [77, 146-148]

1.5.4 Wood-based biopolymers as 3D printing inks

Wood is considered as a gift from nature with intrinsic properties of non-toxicity, biodegradability, and biocompatibility. The application of wood-derived biopolymers assisted with 3D printing is an emerging field that offers promising potential to utilize the most abundant and sustainable resources on earth for the development of advanced functional materials. [134, 149] The major components of wood including cellulose, hemicelluloses, and lignin have versatile properties holding the potential in the development of novel materials for different printing techniques. Cellulose and its derivatives such as microcrystalline cellulose, cellulose esters, and cellulose ethers have been widely studied in the fabrication of customized drug delivery devices *via* the HME process and the FDM technique. [150-159] Considering the utilization of cellulose in bioplastics, UPM launched a biocomposite filament with the ingredients of cellulose and PLA in April 2018, which can be perfectly printed both in fine detail and at large scale. Nanocellulose materials originated from wood-derived cellulose in the area of 3D printing gained great interests especially in biomedical applications. [160] In particular, CNF with its intrinsic gel-formability has been formulated into 3D printable inks itself or with other biomaterials. Recently, the CNF-based formulations have been used to fabricate tissue engineering scaffolds and cartilage implants through 3D printing. [77] Hemicelluloses hold great promise as the aiding agents for modifying cellulose surfaces within CNF-based ink formulation. The functionalized hemicelluloses could play a role in cross-linking as a way to enhance the structure fidelity and

mechanical properties. For example, tyramine-conjugated xylan acts as an auxiliary material for CNF-based ink formulation to keep the printed structure well after enzymatic cross-linking in the presence of H_2O_2. [161] Due to the thermoplastic nature of lignin, lignin has been incorporated into ABS for FDM printing. [162] The phenolic lignin polymers with antioxidant activity holds a great potential in the biomedical applications. [163]

2. Hypothesis and objectives of the work

The main hypothesis of this thesis was that wood-based polymers, especially the polysaccharides, could be used in 3D printing for high-value biomedical applications. Thus, under the umbrella of sustainable bioeconomy and the development of highly value-added products, this work was a frontier interdisciplinary study focusing on 3D printable ink formulation utilizing wood-based biopolymers. The targets of this work were planned for developing different types of inks matching the need of various 3D printing techniques in bulk or minor scale.

One main objective of this work was to find an end-use for hemicelluloses in bulk, *i.e.* to develop the filaments containing hemicelluloses. Thus, the PLA, commonly used in FDM 3D printing filaments, was partially replaced by natural biopolymers. The possibility of 3D printing of the newly formulated filaments was to be assessed by FDM 3D printing.

The other main objective of this work was to develop CNF-based hydrogels for DIW 3D printing as the *in vitro* cell culture platform within the scope of biomedical applications, such as for wound healing. Generally, the behavior of cells is modulated by several factors such as stiffness, porosity, and topography. In order to meet the various requirements of the matrices, especially regarding mechanical stiffness and printing resolution, the printed CNF-based scaffolds could be tuned by the addition of auxiliary cross-linkers. In this work, different cross-linkers were to be synthesized from natural protein and wood polysaccharides and investigated in the formulation of CNF-based inks to aid the fabrication of CNF-based scaffolds. Biological tests with cells for studying possible cytotoxicity and biocompatibility of the CNF-based matrices in biomedical applications were the last objective within this workflow.

3. Materials and methods

In this section, the materials and methods used in this thesis work are described. The main materials involving TEMPO-oxidized CNFs and GGM are discussed in the section of Materials. The main characterization methods are discussed in the section of Methods. More details can be found in attached **Papers II-IV**.

3.1 Materials

GGM samples with average weight molecular weight (Mw) of 30 kDa (**Paper II**), 43 kDa (**Paper IV**) and 13 kDa (**Paper IV&V**) were prepared from spruce thermomechanical pulp by a laboratory-scale method modified from Willför and co-workers [122, 164] Spruce dissolving pulp with a hemicellulose content of 4.9 % (**Paper III & V**) was used as a starting material to prepare TEMPO-oxidized CNFs. GelMA used in the work of **Paper III** was synthesized and provided by Australian National Fabrication Facility (ANFF) Material Node. All chemicals were purchased from Sigma-Aldrich, MERCK, or VWR and used without further purification.

3.2 Preparation methods

3.2.1 Ink formulations

Preparation of PLA/GGM composite via *solvent blending* (***Paper II***)

GGM (Mw, 30 kDa) was mixed with PLA to prepare composites through a solvent blending method. A co-solvent system of DMSO and dichloromethane (DCM) with the volume ratio of 20:80 was used. GGM was firstly dissolved in DMSO at 40 °C. DCM was then added as co-solvent followed by the addition of PLA pellets. The concentration for all blends was kept as 10 g of solid material per 100 mL solvent mixture. Ultrasonification was applied for 15 min to ensure homogeneous mixing. The blends in the solvent were stirred at 35 °C overnight. The composites were formed by dropwise precipitation of the mixture into cold ethanol (4 °C). The precipitated composites were collected and dried in a vacuum desiccator (D-6450 Hanau, Heraeus) at 40 °C overnight to remove solvent residues.

Preparation of filaments via *HME* (***Paper II***)

The filaments were extruded and formed by HME process using a NOZTEK pro extruder (UK). The extruder was first pre-heated to 165 °C. A blank sample of PLA pellets was added to the extruder for chamber cleaning. After all the PLA was extruded out of the chamber, the PLA/GGM composite was poured into the barrel for extrusion with a nozzle diameter of 1.7 mm. The extruded

filament was collected and stored as dry for further studies. The extruder chamber was purged with PLA pellets before next batch.

Formulation of hydrogel ink (***Paper III & V***)

The formulation of hydrogel inks was based on the CNF hydrogel. In **Paper III**, the dry powders or the solution of GelMA was mixed with CNF to obtain a homogeneous ink by continuous shaking at 50 °C. In **Paper V**, the dried GGMMA was added into CNF hydrogel followed by heating in a water bath at 50 °C for 5 min and gentle shaking. In both ink formulations of CNF/GelMA and CNF/GGMMA, photo-initiator (Irgacure 2959) with concentration of 0.5 w/v % was added for UV cross-linking.

3.2.2 Preparation of CNFs

TEMPO-mediated oxidation (***Paper III & V***)

The CNF preparation was proceeded according to an optimized protocol established by Saito and Isogai's report. [165] In brief, one gram of cellulose fibers from spruce dissolving pulp was dispersed in 60 mL distilled water and stirred overnight at room temperature. The TEMPO (16 mg, 0.1 mmol/g fiber) and NaBr (100 mg, 1.0 mmol/g fiber) were dissolved in 40 mL distilled water, and were further added into the fiber suspension. The pH value of the pulp suspension was adjusted to 10.0 by the addition of 0.5 M NaOH. The oxidation started by adding the NaClO solution (14 wt. % active chlorine, 10 mmol/g fiber) dropwise within 15 min. The pH of the reaction was maintained at 10.5 by continuously adding 0.5 M NaOH during the reaction. The oxidized fibers were precipitated in ethanol with a ratio of 1:3 (v/v) and thoroughly washed with deionized water by centrifugation and filtration until the conductivity of the filtrate below 4.5 µS/cm. The oxidized fibers were defibrillated using a Rannie 15 type 12.56x homogenizer operated at 600 and 1000 bar for the first and second pass, respectively. The prepared CNFs were stored at 4.0 °C prior to further use.

3.2.3 Synthesis of hemicellulose derivatives

Enzymatically cross-linkable GGM (***Paper IV***)

GGM samples with Mw of 43 kDa and 13 kDa were functionalized with carboxylic groups *via* TEMPO-mediated oxidation prior to tyramine (TA) conjugation. In brief, GGM (2 g) was dissolved in deionized water (400 mL) for reactions at both cold (2-4 °C) and room temperature (23 °C). The reaction started with the addition of TEMPO (4 wt.%, 40 mL) and NaClO (14 wt.% active clorine, 40 mL). The reaction continued for 15 min with controlling pH of the solution at 10 by dropwise adding 0.5 M NaOH. In order to terminate the reaction, 1 M HCl was added to neutralize the solution. The contaminants such as salts and residual reagents were removed by dialysis with a 12-14 kDa membrane tube against deionized water for 3 days. The purified products were

concentrated to the concentration of 25 mg/mL *via* rotary-evaporation for further use. The TA conjugation was conducted with both native GGM and TEMPO-oxidized GGM by a coupling reaction of the carboxylic groups. The N-(3-dimethylaminopropyl)-N'-ethylcarbodiimide hydrochloride / N-hydroxy-succinimide (EDC/NHS) chemistry was applied to activate the carboxylic groups by adding EDC/NHS to GGM and TEMPO-oxidized GGM solutions (25 mg/mL) with a molar ratio of 1.8/1.8/1 for EDC/NHS/COOH. TA dissolved in DMF, and was added after 30 min with a molar ratio of 1.5/1 for TA/COOH. The reaction was carried out for 3 days under the flow of N_2. The GGMTA was obtained by cold ethanol precipitation and vacuum filtration.

UV cross-linkable GGM (***Paper V***)

GGMMA was synthesized by reacting GGM (Mw, 9 kDa) with methacrylic anhydride. Briefly, one gram of GGM was dissolved in 100 mL of deionized water at 50 °C. The varied amount of methacrylic anhydride from 1 to 3 mL was added to obtain different DS of methacrylate on GGM. The reactions continued for 3 h with controlling pH at 8.0 by the addition of 5.0 M NaOH. The GGMMA was purified by dialysis against deionized water with the membrane tube with cut-off of 2 kDa. The GGMMA was obtained by lyophilization and stored as dry and protected from light prior to further use.

3.3 Characterization methods

3.3.1 Chemical structure analyses

Nuclear magnetic resonance (NMR) spectroscopy (***Paper IV & V***)

The native GGM and its derivatives were analyzed by ^{1}H, and ^{13}C NMR measurements at 298 K in either D_2O or DMSO-*d6* on a Bruker AVANCE III spectrometer operating at 500.13 MHz for ^{1}H and 125.77 MHz for ^{13}C. The quantitative ^{13}C experiments were recorded using a 5 mm Z-gradient BBO (Broadband Observe) cryo-probe.

*Gas chromatography (GC) (**Paper IV**)*

The sugar composition and the degree of oxidation of TEMPO-oxidized GGM (DO(COOH)) were determined by GC. According to established method, [166] acid methanolysis was performed using freeze-dried GGM and TEMPO-oxidized GGM solutions in pear-shaped bottles. The samples were subjected to 2 mL of 2 M HCl in methanol, and placed in 100 °C oven for three hours. Excess of HCl was neutralized by adding 200 µL pyridine. The internal standard of 0.1 mg/mL sorbitol and resorcinol in methanol (1 mL) was added to each sample. The samples were dried by nitrogen flow with 50 °C water bath, followed by drying 15 min in a vacuum desiccator at 40 °C. The silylation of samples was conducted with adding pyridine (150 µL), hexamethyldisilane (150 µL), and

trimethylsilyl (70 µL). The silylated samples were left overnight. The supernatant phase was transferred to GC vials. The analyses was carried out using HP-1 column (25 m in length) by the carrier gas of 0.8 mL/min H_2 and with the following column temperature program: 100 °C; 4 °C/min; 180 °C; 12 °C/min; 290 °C (5 min). The results were analyzed using the program of TotalChrom Navigator. The DO(COOH) was calculated by **equation (1)**

$$DO(COOH) = \frac{c(uronic\ acids)}{c(uronic\ acids)+c(sugars)} * 100\ [\%] \quad \textbf{(1)}$$

where c is the molar concentration in mmol/g.

*Elemental analysis (**Paper IV**)*

The tyramine concentration in the GGMTA was measured by the determination of nitrogen content in an organic elemental analyzer (FLASH 2000 CHNS/O, Thermo Fisher Scientific, UK). The samples of 2±0.2 mg were added into tin cups as sample holders. Cysteine and sulfanilimide were used as calibration standards. Based on the nitrogen percentage, N%, the degree of substitution for tyramine (DS(TA)), was calculated by **equation (2)**

$$DS(TA) = \frac{\mathrm{N\%}*(M_{sugar}+DS_{acetyl}*M_{acetyl})}{100*M_N-\mathrm{N\%}*M_{TA}} \quad \textbf{(2)}$$

where DS_{acetyl} is the degree of substitution of acetyl groups in GGM, and molar mass, M, is used for the sugar unit, acetyl, nitrogen and tyramine.

3.3.2 Molar mass determination

Size exclusion chromatography (***Paper IV&V***)

The molar mass of GGM and its derivatives was determined using high performance size exclusion chromatography (HPSEC) with a multi-angle laser light scattering (MALLS) detector (miniDAWN, Wyatt Technology, Santa Barbara, USA) and a refractive index (RI) detector (Shimadzu Corporation, Japan). Milli-Q water was used during analysis. The HPSEC was combined with a two-column in series system, 2 × Ultrahydrogel™ linear 300 mm x 7.8 mm column (Waters, Milford, USA). The specific refractive index increment (dn/dc) value of 0.150 mL/g was applied for GGM. [167]

3.3.3 Surface chemistry

Charge density of CNFs (***Paper III&V***)

Conductometric titration was applied to determine the carboxylate content of the CNFs. HCl (2.0 mL of 0.1 M) and NaCl (1.0 mL of 50 mM) were added to CNF suspension (50 mg, 0.1%, w/v). Then the suspension was stirred for 90 min before titration. The mixture was titrated with 0.1 M NaOH at the rate of 0.1 mL/min and the charge density of the sample was calculated from the conductivity and pH curves. [168, 169]

3.3.4 Thermal properties

Differential scanning calorimetry (DSC) (***Paper II***)

The glass transition temperature (Tg) and melting point (Tm) were investigated by DSC (DSC Q 2000, TA instruments, USA). The PLA/GGM composite and filament samples were tested in a heat/cool/heat cycle at a temperature range of 0 °C to 220 °C with a heating and cooling rate of 10 °C/min in a standard aluminum pan. The sample size was 3 ± 1 mg for both composites and filaments. Nitrogen as a purge gas was used with a constant flow rate of 50 mL/min. The thermograms were analyzed with the TA Instruments Universal 2000 Software.

Thermal gravimetric analysis (TGA) (***Paper II***)

The thermal stability of PLA/GGM blends and filaments was investigated by a Thermal Gravimetric Analyzer (Q600, TA instruments). The samples were pre-dried overnight in a vacuum desiccator at 40 °C before the analysis. The analysis was conducted in nitrogen atmosphere with a heating rate of 10 °C/min from room temperature to 600 °C.

3.3.5 Biopolymer interactions

Quartz crystal microbalance with dissipation monitoring (QCM-D) (***Paper III & V***)

To investigate the adsorption of GelMA or GGMMA on the surface of CNFs, the QCM-D measurements were carried out using the Q-Sense E4 (Biolin Scientific, Sweden) instrument. QCM-D analyses provide the *in-situ* information on the GelMA or GGMMA molecule adsorption to the CNF materials on the quartz crystals and the viscoelastic properties of the absorbing layer. [170] In both studies, PEI with a concentration of 0.2 mg/mL was first purged for 20 min to the instrument chamber to enhance the adsorption of CNF onto the gold-coated quartz crystals. Then, the chamber was rinsed with DI water. Diluted CNF dispersion was then injected into chamber for the adsorption of CNF layer onto the PEI modified sensor followed by rinsing with DI water. Thereafter, the CNF modified sensors were exposed to either GelMA or GGMMA solutions with specific concentrations. The flow rate through the QCM-D chambers was set to 40 µL/min and kept constant during measurements. During adsorption, the oscillation frequency of the crystal increases and deviation from the fundamental frequency (5 MHz) and its over-tones (15, 25, 35, 55, and 75 MHz) are detected. According to the **equation (3)**, the change in frequency (Δf) is proportional to the mass adsorbed per unit surface (Δm).

$$\Delta m = \frac{-C\,\Delta f}{n} \qquad \textbf{(3)}$$

where C is the sensitivity constant (here C = 0.177 mg/m2) and n is the overtone number (here n = 3). **Equation (3)** is valid for thin, rigid, and uniform films, but it underestimates mass for viscoelastic films, when ΔD > 1. [171] Therefore,

the calculated mass values are estimations and should not be considered as absolute values.

3.3.6 Rheological measurements

*Rheology of filaments in molten state (**Paper II**)*

The rheological properties of the PLA/GGM filaments were investigated in molten state. The sample size was approximately one gram. Rheology measurements were carried out to determine the shear viscosity profiles for the filaments at the printing temperature of 175 °C, which is the temperature used during the filament printing. The measurements were conducted with a rotational AR 2000 rheometer (TA instruments, USA), using parallel plate geometry at the shear rate of 0.005 to 200 s^{-1}. The geometry of the plates and the gap between them were 15 and 1 mm, respectively.

Rheology of GGMTA with enzymatic cross-linking (***Paper IV***)

Enzymatic gelation of GGMTA was investigated by running oscillatory measurements with an 8 mm plate-plate at 1 Hz and 4% strain rate. GGMTA solution (100 µL, 80 mg/mL) was mixed with HRP (15.3 µL, 0.6 mg/ml). GGMTA/HRP solution (30 µL) was used for each measurement. While the measurement started, H_2O_2 (4.59 µL, 1 wt.%) was added whereby the change in storage modulus, G', and loss modulus G'' was monitored. The GGMTA gels were additionally subjected to an amplitude sweep (1 Hz, 0.01-100% strain) to define the linear viscoelastic range (LVR) and a frequency sweep (0.01-100 Hz, 4% strain) to verify the stability of the gels.

Rheology of the formulated inks with UV cross-linking (***Paper III & V***)

The rheological profiles of the formulated inks of CNF/GelMA and CNF/GGMMA were studied on a Physica MCR 301 Rheometer (Anton Paar, Austria) with a cone-plate geometry (ø=50 mm and 1°). The shear-thinning property was studied with a shear rate from 0.01 to 100 s^{-1} at room temperature. Oscillatory measurements were conducted to study the impact of UV-aided gelation time with a constant strain and sweep at 1% and 1.5 Hz, respectively. After starting measurement for 2 min, the formulated inks were irradiated with a UV spotlight with an intensity of 10 mW/cm^2 and the change of storage modulus was registered. The LVR was defined by both amplitude sweep (1.5 Hz, 0.01-100% strain) and frequency sweep (1%, 0.01-100 Hz).

3.3.7 Printability by 3D printing techniques

*FDM 3D printing (**Paper II**)*

The manufactured PLA/GGM filaments were tested with FDM 3D printing using a Me3D desktop printer (Australia) The scaffold prototypes were

designed and printed by the control of 'MatterControl' software as stereolithography files (.stl). The dimensions of the scaffolds were 20 mm in length, 20 mm in width, and 2 mm in height (10 layers). The printing parameters are listed in **Table 3.1**.

*DIW 3D printing (**Paper III & V**)*

3D scaffolds and prototypes were fabricated with a customized 3D printer KIMM SPS1000 Bioplotter (Machtronics 4 Technology, Korea) controlled by a pneumatic dispensing head with a pressure regulator (AD 3000C, Iwashita Engineering, Japan) for CNF/GelMA inks and a 3D bioprinter Rokit INVIVO (South Korea) equipped with screw-driven extrusion nozzle for CNF/GGMMA hydrogel ink. The KIMM Bioplotter software and Creator K software were used to produce a G-code file for printing. The formulated inks were transferred to a syringe as the ink reservoir. Precision tips (27 GA, and 30 GA, Nordson EFD, USA) were used as the dispensing nozzles. $CaCl_2$ solution with the concentration of 5% was added dropwise on the substrate to aid the printing. UV (365 nm) irradiation with intensity of 10 mW/cm^2 for 5 min was applied to cross-link the printed objects. The printing parameters are listed in **Table 3.1**.

***Table 3.1.** Summary of the printing parameters for the formulated inks with different* 3D printing techniques.

Printing technique	FDM	Pneumatic DIW	Screw-driven DIW
Printer	Me 3D	KIMM	Rokit INVIVO
Inks	PLA/GGM filament	CNF/GelMA	CNF/GGMMA
Temperature	175 °C	Room temperature	Room temperature
Printing speed	15 mm/s (1st layer) 20 mm/s	16-34 mm/s	5 mm/s
Driving force	-	65-80 kPa	Input flow 120%
Requirement of the inks	Diameter 1.75±0.15 mm	Homogeneous hydrogel inks with shear-thinning property	
Others	Cooling fan	UV light source	UV light source

3.3.8 Morphological properties

*Atomic force microscopy (AFM) (**Paper III & V**)*

The morphology of CNF and GGMMA anchored CNF was studied by a multi mode 8 atomic force microscopy equipped with a NanoScope V controller (Bruker Corporation, Billerica, MA). Tapping mode in air using NCHV-A probes (Bruker) with a tip radius around 10 nm was applied. Flattening was the only correction while analyzing the images with NanoScope 8.15 software (Bruker). The surface Young's modulus of 3D printed CNF/GelMA scaffolds

were measured using a JPK Nanowizard II AFM (JPK Instruments AG, Berlin, Germany). Force measurements were performed in PBS using a DNP-S10 silicon nitride cantilever (spring constant around 0.06 N/m) with a 10 nm round tip. The spring constant of each cantilever was calibrated before use. Three separate scaffolds were analyzed for each material.

*Optical microscopy (**Paper III**)*

The microscopic images of the printed CNF/GelMA scaffolds were observed using a LEICA M205A optical microscope. The filament diameter was calculated on the average of twenty filaments among the printed scaffolds.

*Scanning electron microscopy (SEM) (**Paper II, III & V**)*

In order to obtain the morphology of the printed scaffolds with the PLA/GGM filaments and CNF/GelMA inks, a scanning electron microscope (SEM LEO Gemini 1530 with a ThermoNORAN Vantage X-ray analyzing system manufactured by Thermo Scientific, Germany) was used. A thin carbon coating was applied onto the sample to make it more electrically conductive. The microscope was operated in a secondary electron mode at an accelerating voltage of 2.7 kV for imaging with an aperture size of 60 μm.

*Confocal microscopy (**Paper III**)*

Confocal images of cell culture with CNF/GelMA inks were acquired at room temperature using Zeiss Zen software on a Zeiss LSM780 confocal laser scanning microscope (Carl Zeiss, Inc.) with Plan-Apochromat 20x. The fluorochromes of Alexa Fluor 546 and 405 were used.

3.3.9 Mechanical properties

*Three-point bending test (**Paper II**)*

Flexural strength of the PLA/GGM filaments was measured. Flexural strength was studied by the three-point bending test according to the *ASTM D790* standard method. The filaments with a diameter around of 1.75±0.15 mm were cut to 30 mm long pieces for flexural test using an instrument of LLOYD LR30K plus (UK) operated at a cross-head speed of 10 mm/min.

*Compressive Young's modulus (**Paper III & V**)*

The compressive strength was conducted with both the cast discs from all the hydrogel inks and the printed scaffolds using CNF/GelMA inks with a Shimadzu EZ-L universal testing machine with a 10 N load cell. The compression speed was set with a constant rate of 0.5 mm/min. The compressive Young's modulus was calculated according to the **equation (4)**:

$$E = \frac{F \times L_0}{A \times \Delta L} \quad \textbf{(4)}$$

where, F is the recorded compressive force, L_0 is the original height of scaffold, A is the area of scaffold contacted with upper compression plate, and ΔL was set with a constant displacement of 2 mm.

3.3.10 Biocompatibility of CNF-based scaffolds

*Cytotoxicity test (**Paper III**)*

The 3T3 fibroblast cells were seeded at a density of 1×10^5 cells per piece of sample in 24-well plates. Once the cell suspension had been in contact with the CNF/GelMA matrix for 12 h, non-adherent cells were washed off and the plate were frozen for 30 min at −70 °C. The plates were then thawed, and cells were stained in 0.5% crystal violet dye for 20 min. After washing, samples were fixed with methanol for 20 min, and then measured at 570 nm. Cytotoxicity evaluation of 3D matrix was performed after 24 h of cell incubation using the MTT kit (Sigma) according to supplier's manual. The plates were immediately measured at 570 nm with wavelength higher than 650 nm as reference using the microplate reader.

*Cell proliferation test (**Paper III**)*

For *in vitro* proliferation assays, 3T3 fibroblast cells were incubated with the 3D matrix in the cell culture medium for 72 h. Then cells samples were fixed with 3.7% paraformaldehyde for 30 min and mixture of acetone and methanol (1:1) for 5 min in ice. Triton X (0.2%) in PBS was used to permeabilize the cell membranes, and the 10% FBS in Triton X-100 and PBS was used for blocking for 2 h. The cells were stained with Phalloidin conjugated with Alexa Fluor 546 for 3 h, and counterstained with DAPI blue for 5 min before mounting on the glass slides. Confocal images were acquired for the prepared assays.

*Statistical analysis (**Paper III**)*

The results on cell studies are expressed as the mean ± STDEV. Comparisons between two groups were analyzed by two-tailed t tests. Comparisons between multiple groups were analyzed by 1-way ANOVA. $P<0.05$ was considered significant. Statistical differences were calculated with the two-tailed unpaired t-test and differences were considered significant at $p\leq0.05$.

4. Results and discussion

4.1 Summary and overview of the thesis work

The overall objective of this work was to study the feasibility to utilize the wood-derived biopolymers such as hemicelluloses and cellulose nanofibrils with emerging state-of-the-art 3D printing techniques, as schematically illustrated in **Figure 4.1**. Moreover, the methodologies for productive ink formulation and facile modification were established to better tune the mechanical properties of those wood-derived biopolymers towards biomedical applications.

The specific workflows of the thesis are as follows:

1) Investigation on the direct utilization of side-stream hemicelluloses in bulk as the replacing materials for PLA in the preparation of FDM printing feedstock materials
2) Development of bioactive CNF-based inks by incorporation GelMA for DIW 3D printing
3) Synthesis of cross-linkers based on GGM by chemical modification
4) Assembly of biomimetic inks with all-wood-derived biopolymers as a platform material towards biomedical applications
5) Investigation of the biocompatibility of the printed CNF-based scaffolds

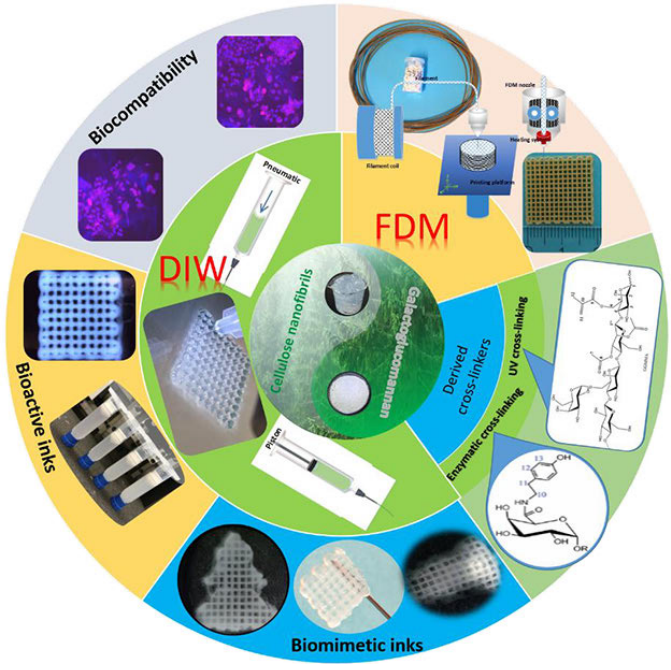

Figure 4.1. *Overview of the thesis work.*

4.2 Polymer blends of PLA/GGM for FDM 3D printing (Paper II)

PLA has been considered as one of the most commonly used biomaterials in the biofabrication of biomedical devices, including surgical sutures, orthopedic fixation implants, drug delivery devices, and tissue engineering scaffolds. [172, 173] PLA is widely used as filament materials for FDM 3D printing. However, PLA as a synthetic polymer, derived from fermented starch mainly using corn, is generating the ethical concern on the global food crisis. Hemicelluloses, the second most abundant polysaccharides after cellulose, are still treated as a side-stream product in biomass processing industries. GGM is the major hemicellulose type in softwoods, and accounts for up to 25 wt.% in Norway spruce species. With the development of novel biorefineries, a recently developed technology enables the access to the water-soluble and polymeric hemicellulose in high purity and abundance. [174] Thus, a strategy to blend economically feasible wood polysaccharides with PLA providing an alternatively sustainable approach to partially replace PLA in feedstock filaments for FDM 3D printing was proposed. The proposed methodology is illustrated in **Figure 4.2**. A solvent blending approach for evenly mixing GGM and PLA was established. The PLA/GGM filaments were manufactured *via* the HME process. PLA could be replaced with as much as 25 wt.% GGM. Importantly, similar mechanical property could be maintained when 20 wt.% GGM was incorporated compared to pure PLA.

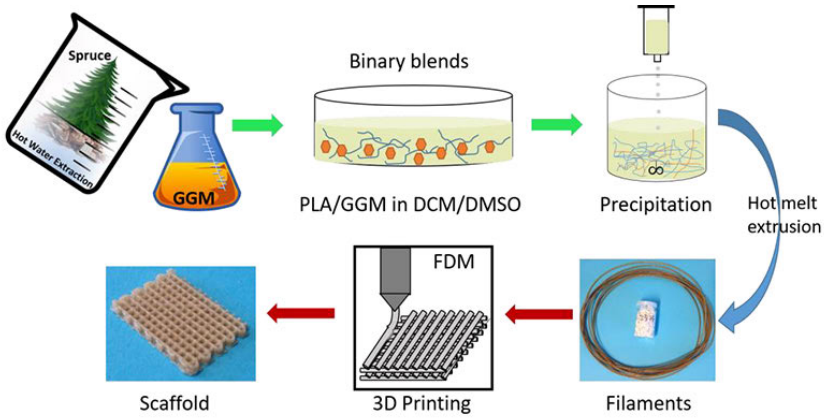

Figure 4.2. *Illustration of FDM 3D printing of PLA/GGM blends from mixing two polymers to filament manufacture, and to scaffold printing.*

4.2.1 Preparation of the filaments of PLA/GGM blends

A solvent blending method was established to evenly mix two polymers by using a co-solvent system of DCM and DMSO, as shown in **Figure 4.3a**. It is well known that the solvents of H_2O, DMSO, and DMF are suitable to dissolve GGM. However, these solvents were not able to dissolve PLA. PLA is soluble in *e.g.* chloroform, DCM, and THF. Considering solvent miscibility, a cost-

effective and efficient solvent mixture of DCM and DMSO was established to dissolve both PLA and GGM. PLA/GGM blends were obtained by subjecting the blend dispersions dropwise to cold ethanol (4 °C). The polymer blends were then dried to remove all the solvents prior to the HME process. All the produced PLA/GGM blends are listed below in **Table 4.1**. The color of the obtained polymer blends was changed from white to slightly yellowish with the addition of GGM (**Figure 4.3b**).

Table 4.1. *Blending ratio between GGM and PLA, and the preparation condition.*

Blend codes[#]	GGM (wt.%)	PLA (wt.%)	Solvent
100P	0	100	DMSO:DCM 20:80
0199	1	99	
0595	5	95	
1090	10	90	
1585	15	85	
2080	20	80	
2575	25	75	

[#] The polymer blends from solvent blending are coded according to the list and thereafter extruded filaments with suffix '-Fila'.

Figure 4.3. *(a) The picture of homogeneous mixture of GGM and PLA with its ratio of 20:80, (b) The precipitated and dried PLA/GGM blends with different compositional ratio, and (c) The formulated PLA/GGM filaments from bottom to top with blends of 100P, 0199, 0595, 1090, 1585, 2080, and 2575, respectively.*

The dried blends were further extruded into filaments by the HME process. Different temperatures in the range of 155-205 °C were tested. Filaments with a stable shape and well-defined diameters in the range of 1.75±0.15 mm were obtained when the extrusion temperature was 165 °C. The color of the filament changed from transparent to brownish color with the addition of 25 wt.% GGM (as observed in **Figure 4.3c**). In these formulations, no color additives were added. Therefore, it was assumed that a small amount of aromatic residues in GGM were oxidized during extrusion and caused the color change of the extruded filaments. [122, 124]

4.2.2 Thermal behavior of the filaments

Thermal properties including Tg, Tm, thermal degradation, and thermal rheology of the materials are crucial for FDM 3D printing. The determination of Tg would be more sensitive after erasing the thermal history of the polymer blend material by the first run of heating. Thus, a heat-cool-heat run was applied for DSC analysis. According to **Figure 4.4a and 4b**, no obvious change of Tg both in polymer blends and filaments were detected after second heating run. Only one Tg of 62 °C was observed for all the polymer blends material referring to the Tg of PLA. [175] However, the influence of GGM on melting behavior is more reflected by the second heating thermograms of the filaments with two obvious melting peaks. As shown in **Figure 4.4b**, the filaments could be molten when the temperature was 155-170 °C. The melting peaks at lower temperature (around 155 °C) were more extensive than the peaks at higher temperature (around 165 °C). This might be associated with the melting progression of PLA crystals with different sizes. [176] When the ratio of GGM reached 25 wt.%, only one broad melting peak appeared due to the formation of a broad distribution of PLA crystal size by the addition of the large amount of GGM. Considering the temperature for printing, it was overall balanced from melting and degradation temperature. In another word, the printing temperature must be higher than the melting temperature and lower than the degradation temperature. According to **Figure 4.4c**, the addition of GGM to PLA matrix caused a decrease of thermal stability of the filaments. All the PLA/GGM filaments started to degrade around 160 °C while the severe decomposition happened at a temperature of 260 °C. In order to make an easy melt-flow without clogging the printing nozzle and less material degradation, the printing temperature was set at 175 °C. **Figure 4.4d** reveals the general shear-thinning profile of the PLA/GGM filaments under the molten state at 175 °C, which is mostly required for the extrusion-based printing technique.

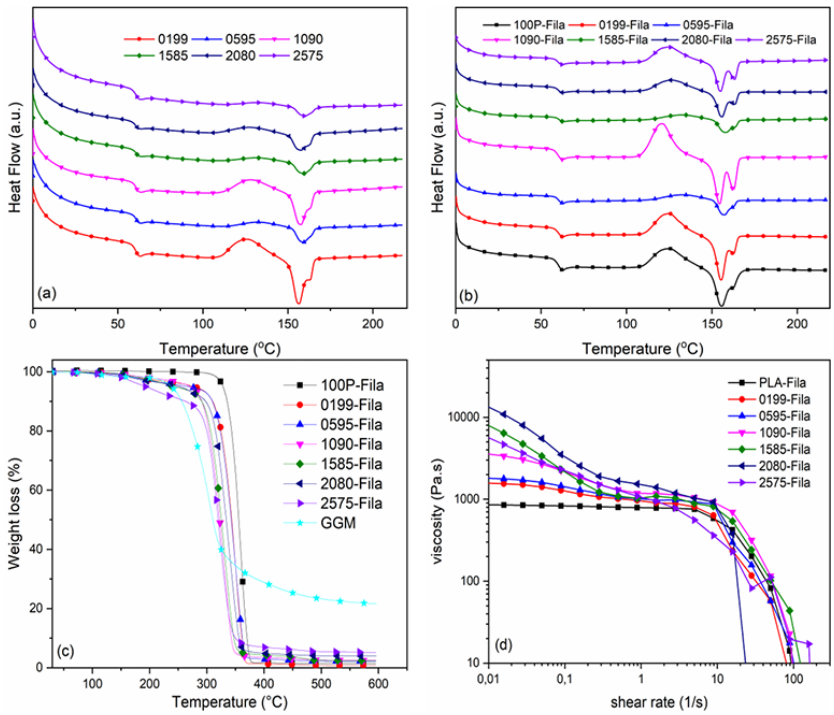

Figure 4.4. *DSC thermograms of the second heating run of PLA/GGM blends (a) and filaments (b), thermal decomposition curves of filaments (c), and rheology curves of filaments at printing temperature of 175 °C (d). Note: PLA-Fila stands for the filament directly extruded from commercial PLA pellets. The codes of polymer blends are listed in Table 4.1 and the relevant filaments with suffix '-Fila'. Images were adapted from Paper II with Copyright (2018) ELSVIER.*

4.2.3 Mechanical properties of the PLA/GGM filaments

During the printing process, the filament is first fed into a liquefier and then the molten ink is pushed through the nozzle like a piston. During this process, the filaments tend to be bent or buckled, which is governed by flexural modulus. [140, 177] Thus, flexural strength is a vital factor for the success of the filament feeding and printing. Compared to the flexural modulus of the neat PLA around 3.2±0.3 GPa, the flexural moduli of the PLA/GGM filaments had similar values (**Figure 4.5**). However, the PLA/GGM filament of 2575-Fila showed a rather low value. This might be due to that the relative large amount of GGM (25 wt.%) impeded the PLA polymer chain entanglement and caused intermolecular phase separation.

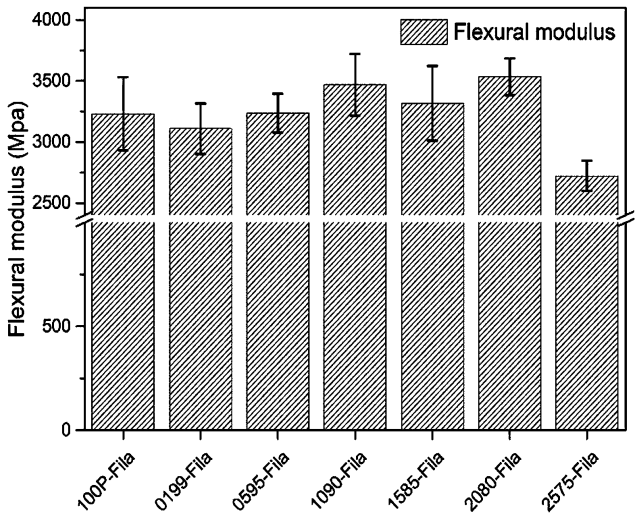

Figure 4.5. *Flexural modulus of PLA/GGM filaments from three-point bending tests. Image was adapted from Paper II with Copyright (2018) ELSVIER.*

4.2.4 Scaffold printing with PLA/GGM filaments

Scaffolds were successfully printed with the formulated PLA/GGM filaments (shown in **Figure 4.6**). The success is determined not only by thermal and mechanical properties of the filaments but also by other parameters such as the diameter of the filament and printing speed. Importantly, a suitable dimeter of the filament is essential for the continuous feeding and printing. According to our experience, the filament diameter in the range of 1.75±0.15 mm would be suitable for the printer with the default requirement for the filament diameter of 1.75 mm. The printing speed significantly affects the resolution of the printed scaffold. It is worth to mention that the speed of the first layer plays a significant role in determining the quality of the whole object.

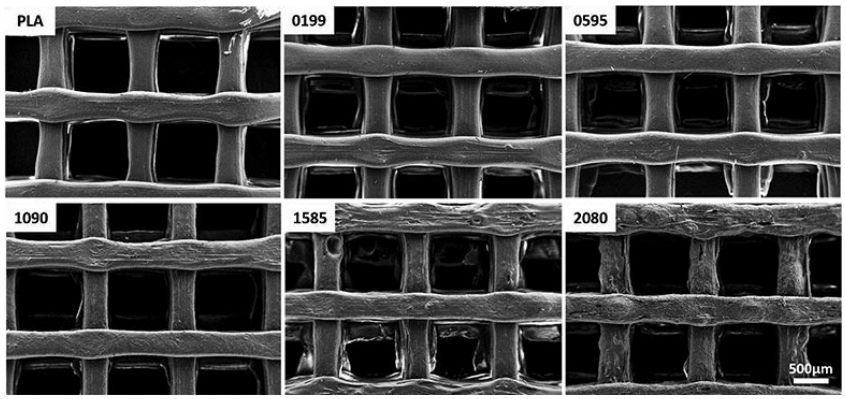

Figure 4.6. *SEM images of the 3D printed scaffold from different PLA/GGM filaments from PLA, 0199, 0595, 1090, 1585, and 2080, with a scale bar of 500 µm. Images were adapted from Paper II with Copyright (2018) ELSVIER.*

4.3 CNF/GelMA ink formulations for DIW 3D printing (Paper III)

CNFs in the form of hydrogel stand out as a platform biomaterial in ink formulation due to their shear-thinning property, low cytotoxicity, good mechanical property, and structural similarity to ECM. [134, 149] However, the printing of only CNFs has a critical challenge in shape fidelity. [77, 178] Cross-linking strategies need to be applied during or after printing. In one of our studies, the structural stability of CNF-based was obviously improved by chemical cross-linking of CNFs with BDDE after the printing of the whole objects. [179] Nevertheless, auxiliary materials are also preferable to be incorporated into CNF-based ink formulation to keep the geometry stability after cross-linking of the auxiliary materials. The auxiliary materials can be natural or synthetic polymers, which are amenable to be ionic, photochemical, or thermal cross-linking. [77, 180, 181] For example, alginate was commonly integrated in formulating CNF-based inks due to its possibility of being easily and rapidly cross-linked by divalent ions such as Ca^{2+}. [77] In this section, GelMA was used as an auxiliary material in the CNF-based ink formulation *via* UV-aided cross-linking. GelMA as a derivative of collagen supplies cell binding motifs such as arginine-glycine-aspartic acid (RGD) peptides, which could improve the cell responses. [21, 182] This study presents a low-concentration ink formulation with 1 w/v % TEMPO-oxidized CNFs and less than 1 w/v % GelMA. The presence of TEMPO-oxidized CNFs facilitated the UV cross-linking of GelMA under relatively low concentration of less than 1 w/v %. By tuning the compositional ratio between CNFs and GelMA, the compressive Young's modulus of the printed scaffold could be well tuned. Last but not least, high-resolution scaffolds of CNF/GelMA were successfully printed with high fidelity and stability through DIW 3D printing assisted by UV post curing. **Figure 4.7** illustrates DIW 3D printing of low-concentration inks with TEMPO-oxidized CNFs and GelMA.

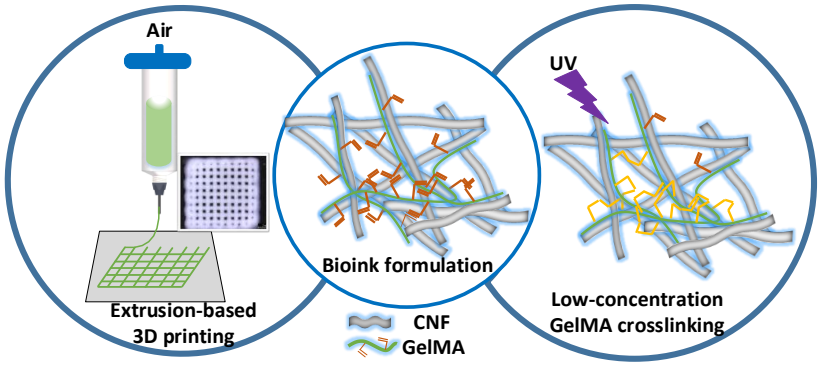

Figure 4.7. *Illustration of the ink formulations with CNF/GelMA for obtaining lightweight scaffolds* via *DIW 3D printing with assistance of UV cross-linking.*

4.3.1 Ink formulation of CNFs and GelMA

It is of vital importance to understand the polymer interaction between CNFs and GelMA in order to obtain the ink homogeneity for further good printability. The polymeric interaction between CNFs and GelMA was studied *in situ* through QCM-D measurements. As indicated in **Figure 4.8a**, the GelMA was strongly adsorbed on the CNF layer. Compared with 0.5 w/v % gelatin as the reference with the absorbed mass of 75 mg/m^2 in QCM-D studies, the adsorption of GelMA with different concentrations from 0.2 w/v % to 1.0 w/v % resulted in the adsorbed mass amount from 115 to 180 mg/m^2 (**Figure 4.8b**). However, a saturated adsorption tendency was observed when the GelMA amount was increased form 0.5 w/v % to 1.0 w/v %. It indicates the concentration limitation of GelMA being less than 1w/v % could therefore be incorporated during ink formulation. This was revealed by the phase separation phenomenon while more than 1w/v % of GelMA was incorporated into the ink formulation. Thus, dry powder of GelMA was added into 1 w/v % CNF hydrogel resulting in 0.2 w/v % and 0.5 w/v % final GelMA concentrations, respectively, for the ink of CNF:GelMA=5:1 and 2:1. In order to avoid the clogging of dispensing tips during printing, 10 w/v % of GelMA solution was added to 1 w/v % CNFs resulting in 1 w/v % GelMA final concentration and 0.9 w/v% CNF final concentration for ink formulation of CNF:GelMA=9:10. The ink formulation with CNFs and GelMA was shown in **Table 4.2**.

Table 4.2. *Ink formulation of CNF/GelMA, and printing parameters for the formulated bioinks.*

Ink code	CNFs (w/v %)	GelMA (w/v %)	Tip size (G)	Pressure (kPa)	Speed (mm/min)
CNF	1	-	27	70	1000
CNF:GelMA=5:1	1	0.2	30	65	2000
CNF:GelMA=2:1	1	0.5	30	70	2000
CNF:GelMA=9:10	0.9	1	30	80	2000

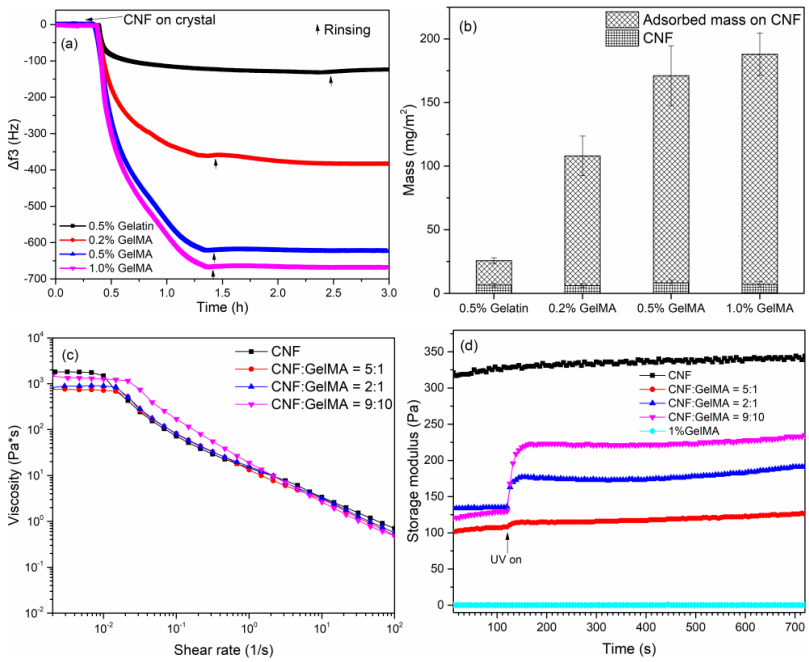

Figure 4.8. *(a) QCM-D adsorption curves of GelMA onto CNF layer, (b) Adsorbed GelMA mass on the CNF layer, (c) Viscosity property of the formulated CNF/GelMA bioinks, and (d) Storage modulus of the formulated bioinks before and after UV irradiation, with UV switched on at 120 s.*

The shear-thinning behavior of CNF/GelMA was recorded as shown in **Figure 4.8c**. As well known, CNFs intrinsically show shear-thinning property. [49, 154] Thus, the incorporation of GelMA did not change their yield-flow behavior. However, the zero-shear viscosity plateau was prolonged by the addition of more GelMA. The plateau also decreased in the presence of GelMA due to the macromolecular interaction as indicated by QCM-D measurements. Based on that, the ink flow became easy when GelMA was incorporated. The success of UV cross-linking was demonstrated by applying UV irradiation at 120 s during oscillatory measurements on the formulated inks. According to **Figure 4.8d**, the storage moduli of the formulated inks rapidly increased immediately after turning on the UV light followed by a level-off plateau. The time difference between these two points is considered as the required cross-linking time. The rate of cross-linking plays a significant role in biofabrication requiring a short gelation window. [183] For all the formulated inks, the required cross-linking time was as short as within 30 s. According to a recent study by O'Connell and co-workers, [183] no clear cross-linking phenomenon was observed when the GelMA concentration was below 2.5 w/v %. As shown in **Figure 4.8d**, the viscoelasticity of only 1 w/v % GelMA and 1 w/v % CNF did not change with UV irradiation. This indirectly reveals that the presence of TEMPO-oxidized CNF could play a key role in facilitating cross-linking of low-concentration GelMA (less than 1 w/v %).

4.3.2 Printability and morphology of the scaffolds

The printability and shape fidelity of the formulated hydrogel inks were investigated with a DIW 3D printer assisted by a pneumatic dispensing control. The images of the printed scaffolds are shown in **Figure 4.9** after screening of different parameters including printing speed, extrusion pressure, and tip diameter (**Table 4.2**). The same printing speed at 2000 mm/min was applied throughout this study. The diameter of the designed struts for each scaffolds was controlled in the range of 0.25±0.01 mm *via* tuning the pneumatic pressure between 60 to 80 kPa. The diameter of dispensing tips was reduced from 27 GA (ø=0.2 mm) for the printing of only CNF ink to 30 GA (ø=0.15 mm) for the CNF/GelMA inks. This is because the adsorption of GelMA on CNF makes the flow through the tip easier as the decreased zero-shear viscosity of the formulated ink indicated in **Figure 4.8c**.

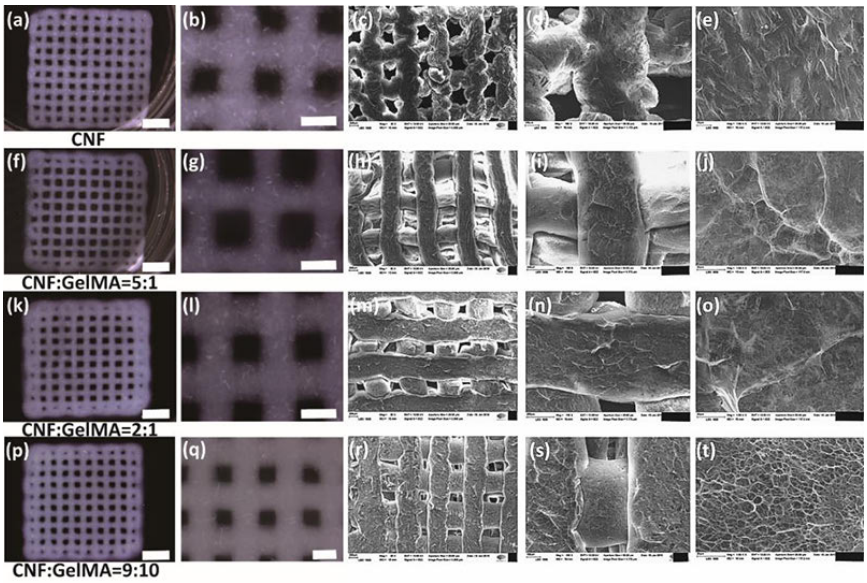

Figure 4.9. *Morphology images of the printed scaffolds from optical microscope (left two columns) and scanning electron microscope (right three columns), the images in the same column have same scale bar with 2 mm (a, f, k, p), 500 µm (b, g, l, q), 200 µm (c, h, m, r), 100 µm (d, i, n, s), and 20 µm (e, j, o, t) from left to right column.*

The morphology of the freeze-dried scaffolds was investigated by SEM, as shown in **Figure 4.9**. For CNF scaffolds, the struts did not straightly align as they originally displayed in wet status. The pores severely deformed without keeping the resolution. At high magnification, the image of the CNF scaffold in **Figure 4.9e** shows large CNF fibril bundles and aggregates due to the presence of the strong hydrogen bonds. However, the struts in the freeze-dried scaffolds of CNF/GelMA (**Figure 4.9i, n, and s**) were aligned more straight, and the surface of the struts became smoother compared to that of CNF (**Figure 4.9d**).

Moreover, the distinctive network appeared on the surface of scaffolds with the addition of more GelMA (**Figure 4.9j, o, and t**) instead of the only shown fibril bundles. This might be attributed to the adsorption of GelMA on CNF, which inhibited the formation of hydrogen bonding between CNFs and further resulted in an impact on guiding the fibril orientation. [184] As shown in the scaffold of CNF:GelMA=9:10 (**Figure 4.9t**), the surface of the printed strut with a microporous structure is regarded as a benefit for cell attachment and proliferation during *in vivo* conditions by improving diffusion into and out the scaffolds. [185]

4.3.3 Mechanical properties of the CNF/GelMA scaffolds

The compressive Young's modulus was evaluated by the compression tests on both the cast discs and printed scaffolds of the formulated inks (**Figure 4.10a**).The compressive Young's moduli of the cast discs varied from 2.3 kPa to 4.5 kPa when the content of GelMA increased. This could be attributed to the increased solid content load [178] and cross-linked GelMA network. The compressive Young's modulus of the printed scaffolds followed that of cast discs with an increasing tendency by the addition of more GelMA. The difference of compressive Young's modulus between the cast discs and the printed scaffolds might be attributed to the difference in the porosity. Furthermore, the local surface stiffness of the printed scaffolds was assessed by AFM, as shown in **Figure 4.10b**. The surface Young's modulus followed the same trend as the compressive Young's modulus of both cast discs and printed scaffolds. The average surface Young's modulus increased from 400 to 700 Pa with the increase of GelMA content. The surface stiffness of the printed scaffolds of CNF/GelMA mainly corresponds to the varied cross-linking of GelMA incorporated in the scaffolds.

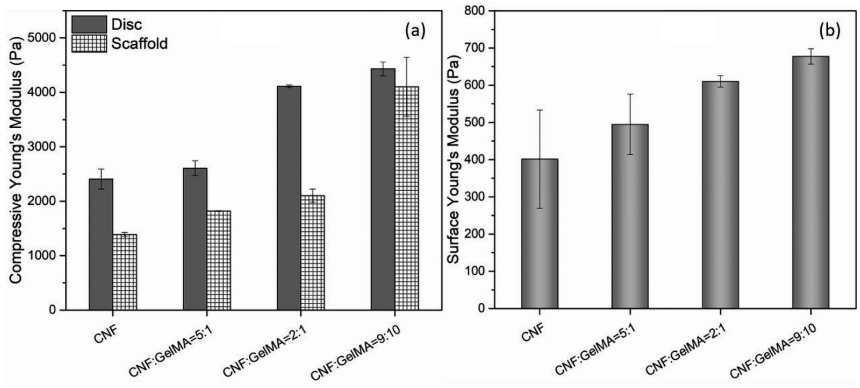

Figure 4.10. *(a) Compressive Young's modulus for the cast disc and printed scaffolds, and (b) Local surface stiffness of the strut on printed scaffolds measured by AFM.*

4.4 Cross-linkable GGM for hydrogel preparation (Paper IV & V)

GGM from spruce consists of a backbone of randomly distributed (1→4)-linked mannose and glucose units with side chain of (1→6)-linked galactose units linked to mannose. All the monomer units of GGM are pyranose containing free hydroxyl groups at the positions of 2, 3 and 6. In this section, the free hydroxyl groups are utilized to be functionalized with either tyramine or methacrylate groups, resulting in the products of GGMTA or GGMMA (**Figure 4.11**), respectively. For the synthesis of GGMTA, GGM was first oxidized to introduce carboxylic groups through TEMPO-mediated oxidation, which is essential for further amine coupling with tyramine. The synthesis of GGMMA is a one-step aqueous reaction with methacrylic anhydride by controlling pH and temperature. After synthesis, the possibility of being cross-linked with GGMTA and GGMMA was investigated by enzymatic and UV-induced cross-linking, respectively.

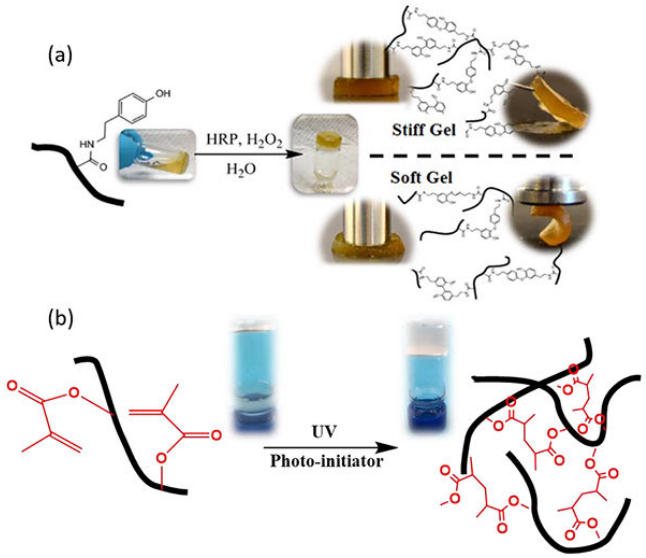

Figure 4.11. *Illustration of the gelation of GGM derivatives. (a) Gelation of a GGMTA sample visualized by tilting and examining how the solution turns into the gel form, which stops flowing in the presence of HRP and H_2O_2; and (b) The gelation of a GGMMA sample by exposing to UV light in the presence of a photo-initiator. Image (a) was adapted from Paper III with Copyright (2017) ELSVIER.*

4.4.1 Synthesis of cross-linkable GGM

Synthesis of GGMTA

Two GGM samples (Mw 43 kDa and 13 kDa) were used for the TEMPO-mediated oxidation at different temperatures (2-4 °C and 23 °C). GGM

carboxylate derivatives with different degrees of oxidation and molar mass are presented in **Table 4.3**. The chain scission of GGM happened independently after TEMPO-oxidation, which is comparable to the studies on how reaction conditions during TEMPO oxidation affect the molar mass of GGM. [186, 187]

***Table 4.3**. Summary of GGM and their chemical derivatives presented with their respective molecular weights. DO(COOH) is given for the degree of oxidation in TEMPO-oxidized GGM, and DS(TA) is presented for the degree of substitution for tyramine.*

Native GGM		TEMPO oxidized GGM				GGMTA			
Code	Mw (kDa)[a]	Sample	T (˚C)	Mw (kDa)[a]	DO(COOH)[b]	Sample	Mw (kDa)[a]	DS(TA)	N (wt.%)[c]
H-0	43	H-0	-	-	0.04	H-0T	63	0.01	0.7
		H-1	2-4	12	0.34	H-1T	30	0.18	1.6
		H-2	23	14	0.63	H-2T	37	0.27	2.9
L-0	13	L-1	2-4	7.7	0.17	L-1T	22	0.07	1.3
		L-2	23	9.5	0.49	-	-	-	-

[a] Molar mass determined by HPSEC, [b] Degree of oxidation based GC data, and [c] Percentage of nitrogen in each sample measured by elemental analysis.

The synthesis of GGMTA was illustrated in **Figure 4.12a**. The presence of tyramine on the GGM was investigated by NMR. The signals of the proton NMR (**Figure 4.12b**) from GGM coincide with previous work, [117] where the anomeric proton (H1) of GGM gave signals for all samples at δ 4.4-5.6 ppm and the remaining protons from GGM (H2-6) at the peak region δ 3.2-4.4 ppm. For the ^{1}H NMR of GGMTA, the distinctive peaks at δ 6.6-7.0 ppm representing tyramine groups were assigned with H12 and H13, which could not be found in the native GGM and TEMPO-oxidized GGM. The DEPT-135 NMR (**Figure 4.12c**) spectra verified the introduction of tyramine with the existence of C10 and C11 only in the GGMTA samples. The DS(TA) was calculated from the nitrogen content of bound tyramine as measured by elemental analysis. Comparing the DS(TA) with DO(COOH), it is notable that the introduction of tyramine could be controlled by the oxidation of GGM. As a control, tyramine was reacted with native GGM resulting in a very low DS(TA) of only 0.01.

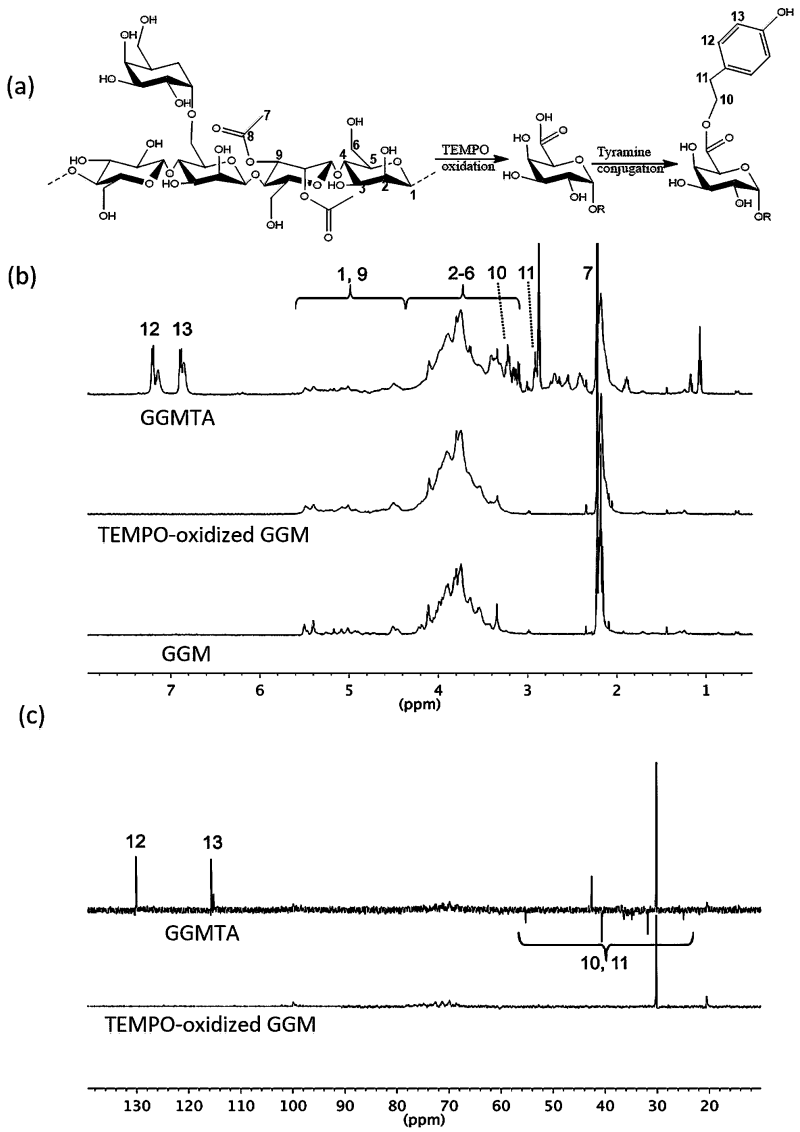

Figure 4.12. *(a) Illustration of the GGMTA synthesis, (b) ^{1}H NMR spectra for native GGM, TEMPO oxidized GGM and GGMTA, and (c) DEPT-135 spectra where the CH_2 peaks of tyramine are identified and the CH_3 signal of DMF is observed. Images were adapted from Paper IV with Copyright (2017) ELSEVIER.*

Synthesis of GGMMA

The synthesis of GGMMA was conducted by reacting GGM with methacrylic anhydride in an aqueous solution under mild alkaline condition at 50 °C instead of using organic solvents and catalysts. [117, 118] The synthesis of GGMMA was illustrated in **Figure 4.13a**. According to **Figure 4.13b**, ^{1}H NMR spectra

of GGMMA dissolved in DMSO-*d*6 confirmed the methacrylation of GGM. The distinctive peaks of the double bond region (δ 5.5-7.0 ppm) and a sharp singlet that corresponded to the methyl groups (δ 1.9 ppm) in the modified GGM chain were registered. To evaluate the influence of methacrylate on cross-linking ability of GGMMA, three GGMMA samples with varied DS of methacrylate (DS(MA)) were synthesized. The DS(MA) was determined by quantitative ^{13}C NMR (**Figure 4.13c**). According to the integral comparison based on the anomeric carbon (δ 95-105 ppm), comparable DS values for the GGMMA samples could be obtained, as shown in **Table 4.4**, from the featured peaks of carbonyl carbon (δ 167 ppm), vinyl carbons (δ 126 and 145 ppm), and methyl carbon (δ 18 ppm), respectively. Additionally, the measured average number molar mass (Mn) of the GGMMAs by HPSEC increased from 9 kDa of GGM to 14 kDa with an increase in DS value.

Table 4.4. *The DS of the esterified methacrylate groups and the average molar mass distribution of the unmodified and GGM and GGMMA materials.*

Code	DS(MA)[a]	Mn/ kDa[b]
GGM	-	9
GGMMA0.18	0.18	11
GGMMA0.25	0.25	14
GGMMA0.40	0.40	14

[a] DS(MA) determined from quantitative ^{13}C NMR, and [b] Mn determined from HPSEC.

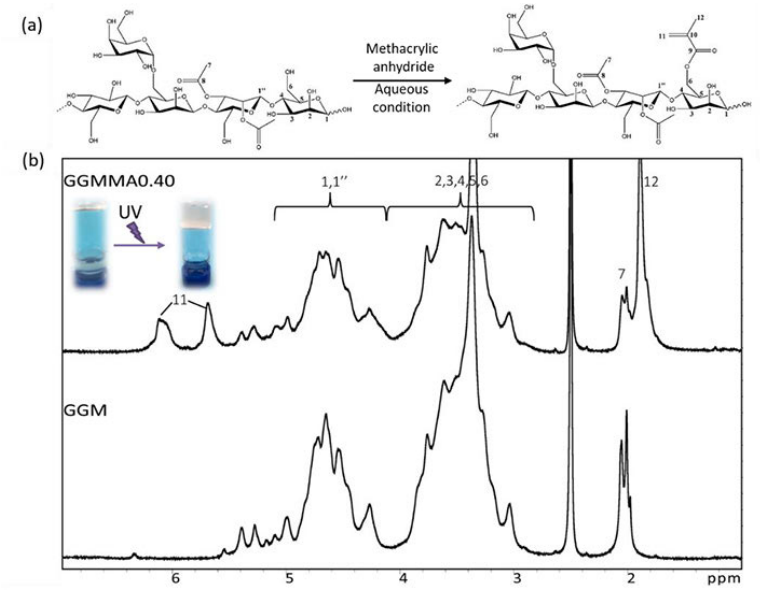

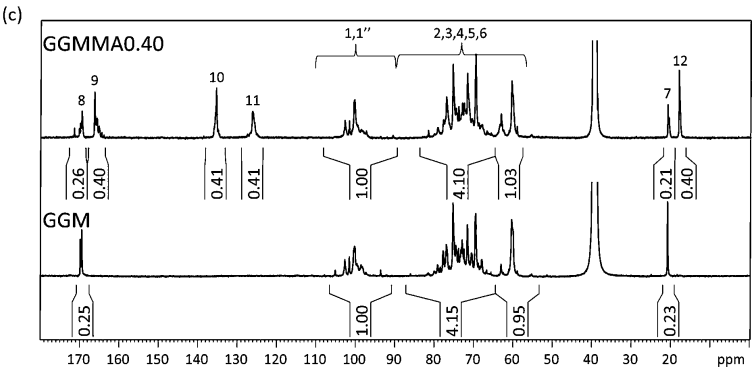

Figure 4.13. *(a) Illustration of GGMMA synthesis, (b) ^{1}H NMR spectra of GGMMA0.40 and native GGM, and (c) Quantitative ^{13}C NMR spectra of GGMMA0.40 and native GGM.*

4.4.2 Cross-linking of GGM derivatives

Enzymatic cross-linking of GGMTA

The gelation possibility of GGMTA was investigated by enzymatic cross-linking with addition of one cross-linking enzyme (Horseradish peroxidase, HRP) and at the presence of H_2O_2. The phenol groups of GGMTA are coupled either by C-C bonds at the ortho-position or by C-O bonds at the ortho-position and the oxygen of the phenolic group. [188] The gelation could be visibly compared whether the solution of GGMTA stopped flowing after the addition of HRP and H_2O_2. The gelation of GGMTA samples of H-1T and H-2T (**Table 4.3**) was successful. However, the GGMTA samples of H-0T and L-1T could not form gels. This could be resulted from the introduced small amount of tyramine groups on the GGMTA sample of H-0T. In the case of the GGMTA sample of L-1T, the failure of gelation might be due to either too low molar mass or too low DS(TA). According to studies regarding other types of tyramine-conjugated hemicelluloses, xylan-conjugated tyramine could be gelated when the DS(TA) of xylan was over 0.08. [119, 189] Nevertheless, the uneven distribution of tyramine groups on the GGM chain could be another reason for the gelation failure due to the uneven distribution of the introduced carboxylic groups by TEMPO-mediated oxidation. The rheology studies of oscillatory measurements were conducted to compare the gelation time of the GGMTA samples of H-1T and H-2T. According to **Figure 4.14**, the gelation happened instantly after the addition of HRP and H_2O_2 as shown by the jump of the recorded moduli. Both of the samples were fully cross-linked in less than 7 minutes, which is indicated by the level-off of the storage modulus (G'). The storage modulus of the GGMTA sample H-2T was higher than H1-T showing the different viscoelastic properties, which is also correlated with the values of DS(TA).

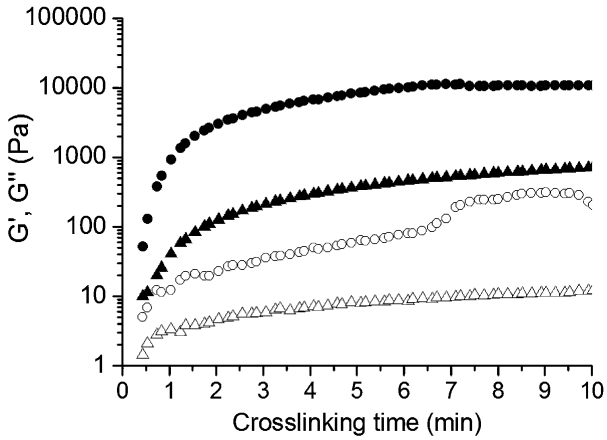

Figure 4.14. *The study of cross-linking time, storage moduli, and loss moduli over time after addition of 1% H_2O_2 at the presence of HRP. Storage modulus, G' (closed symbols), and loss modulus, G'' (open symbols), for H-2T (○) and H-1T (△). Image was adapted from Paper III with Copyright (2017) ELSVIER.*

UV cross-linking of GGMMA

The gelation of GGMMA was demonstrated by exposing the GGMMA solution with the addition of photo-initiator (Irgacure 2959) to UV light source (356 nm). The double bonds in the methacrylate groups are coupled together under the aid of the generated radicals by UV irradiation. [117, 190] The gelation could be visibly observed whether the solution of GGMMAs stopped flowing after the UV irradiation. As shown in **Figure 4.15**, different concentrations of the GGMMA0.25 with 1 wt.%, 2 wt.%, and 3 wt.% were exposed to UV spotlights for 5 min. Both GGMMA0.25 at concentration of 2 wt.% and 3 wt.% successfully formed gels after UV irradiation of 3 min and intensity of 10 mW/cm^2. However, GGMMA with the concentration of 1 wt. % could not form gel when the DS(MA) was below 0.25. According to the above studies of the ink formulation using CNFs and GelMA, the GelMA with concentration less than 1 w/v% could be cross-linked when it was formulated and strongly ionic interaction with CNFs. The intrinsic affinity between GGM and CNFs might increase the possibility of gelation of GGMMA when GGMMA is at a low concentration. Compared with GGMTA, GGMMA requires rather short time for gelation. Therefore, the GGMMA was chosen as a cross-linker in further CNF-based inks for DIW 3D printing.

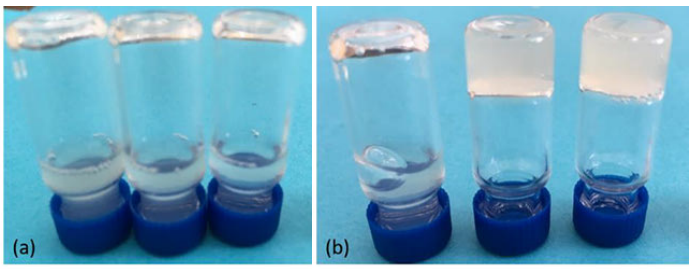

Figure 4.15. *The demonstration of gelation of GGMMA samples before (a) and after (b) UV irradiation. Note: the used GGMMA sample is GMMA0.25 with concentration of 1 wt.%, 2 wt.%, and 3 wt.% from left to right.*

4.5 All wood-based biopolymers for 3D printing (Paper V)

Hemicelluloses and their derivatives could not alone satisfy the needs of the viscosity for 3D printable inks. Thus, they are not able to work as the ink for 3D printing alone. Inspired by the biomimetic perspective, the intrinsic affinity of hemicelluloses to cellulose prompts hemicellulose and their derivatives as the promising candidates to be reinforcing cross-linkers in the development of cellulose-based ink formulation. [191-193] In this section, the synthesized GGMMA was investigated as a cross-linker for the CNF-based ink formulations. The introduction of methacrylate groups on GGM was verified without affecting their intrinsic interaction to CNFs. Different ink formulations were prepared by varying the use of GGMMA with different DS(MA) and different compositional ratio between GGMMA and CNFs. All the ink formulations showed a rapid gelation window, which facilitates the utilization of all wood-based biopolymers as a proper ink for the DIW 3D printing. The printed objects showed an extra-high resolution. Nevertheless, a wide and tunable spectrum of mechanical properties with different formulations could be achieved showing a great potential as a culture platform for different cell lines.

4.5.1 Ink formulation of CNFs and GGMMA

The interaction between GGMMA and CNFs showed an irreversible adsorption behavior by **Figure 4.16a**. The GGMMA tends to be adsorbed in a greater amount of weight on CNFs compared to the native GGM. If the mass change is converted to a change in mole amount (mmol/m^2), the adsorbed amount of GGMMAs was kept on the same level as that of the native GGM. Thus, the methacrylation of GGM did not affect the affinity of GGM to CNFs. This might be due to the remaining strong hydrogen bonding from their similar polymer backbone. The adsorption of GGMMA on CNFs improved the formation of the interpenetrating polymer networks and further offered the mechanical strength of the cross-linked hydrogels. Inks were formulated by directly dissolving GGMMA into CNF hydrogel. Different ink formulations are displayed in **Table 4.5**.

Table 4.5. *Ink formulations with CNFs and GGMMA.*

Ink	CNFs (wt.%)	GGMMA		Compositional ratio between CNFs and GGMMA
		Type	wt.%	
CNF			0	-
IA[a]			1	1:1
IB[a]		GGMMA0.18	2	1:2
IC[a]	1		3	1:3
IIB[b]		GGMMA0.25	2	1:2
IIC[b]			3	1:3
IIIB[c]		GGMMA0.40	2	1:2

Note: [a] Ink formulation with GGMMA0.18, [b] Ink formulation with GGMMA0.25, and [c] Ink formulation with GGMMA0.40.

To investigate the gelation possibility of the formulated inks and the required gelation time, oscillatory measurements with a rheometer was proceeded for all the formulated inks. As shown in **Figure 4.16b**, a clear increase of the storage moduli for all the ink formulations except CNFs immediately after switching on the UV light at 120 s could be observed. All the ink formulations showed a rather rapid gelation window in the range of 1-4 min. When the inks of IA, IB, and IC were compared, the gelation rate tends to be faster when more GGMMA with the same DS(MA) were added. Inks of IB, IIB, and IIIB, which were formulated in the same compositional ratio of 1:2 for CNF/GGMMA but keeping the GGMMA with increased DS(MA), showed similar trends as varying the DS values. Moreover, the G'_{max} of ink formulation with 3 wt.% of GGMMA0.25 and 1 wt.% of CNF reached 60 kPa, which was even higher than that of 17.5 wt.% GelMA. [183] Therefore, the ink formulation of CNF/GGMMA showed a great potential to form a strong and lightweight hydrogel material. By varying the DS(MA) and the addition amounts of GGMMA in the ink formulation, a biomaterial matrix with well-tuned G' was displayed after cross-linking. This indicates that the formulated inks with a tunable strength, mechanical rigidity, and the ability to store deformation energy in an elastic manner. [194]

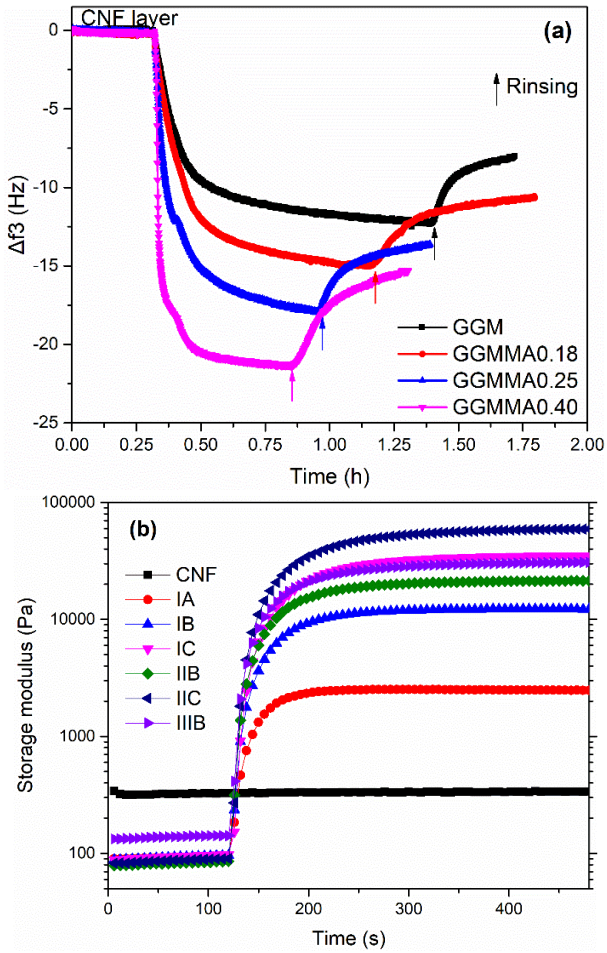

Figure 4.16. *(a) QCM-D adsorption curve of GGMMA onto CNF layer, and (b) Storage moduli profiles of the CNF/GGMMA inks with UV turning on at 120 s. Note: ink of series I with 1 wt.% CNF and GGMMA0.18 with varying compositional ratio to CNF of 1:1, 2:1, and 3:1, respectively, referring to IA, IB, and IC; ink IIB and IIC formulated by 1 wt.% CNFs with 2 wt.% and 3 wt.% GGMMA0.25, respectively; ink IIIB formulated by1 wt.% of CNFs with 2 wt.% GGMMA 0.40.*

4.5.2 Promising culturing platforms for various cell lines

Biologically, the tissue stiffness and the function of native tissue in the body vary greatly and are correlated. [195] Therefore, it is crucial to match the stiffness of the native tissue when engineering tissue equivalents for mimicking the microenvironments of living cells. [196] The compressive Young's moduli of the formulated inks were measured on the cast discs. As shown in **Figure 4.17**, the compressive Young's modulus of the hydrogels prepared from the CNF/GGMMA inks can be tuned in the range of 2.5-22.5 kPa. The wide range of the material stiffness could be designed for the use in specific cell culture.

Thus, the formulated CNF/GGMMA inks showed a promising potential as culture platform in *in vitro* cell study engaging different cell lines, as well as highlighting specific physiological phenomena.

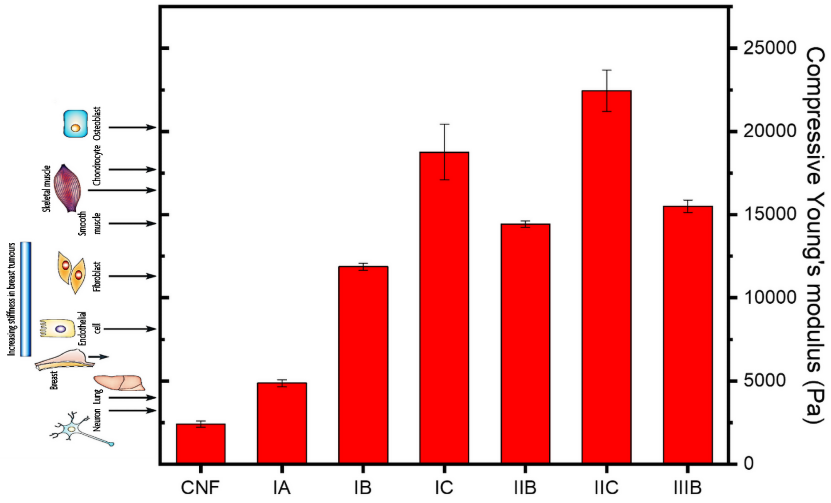

Figure 4.17. *The compressive Young's modulus of the cast discs with different CNF/GGMMA ink formulations. Cell images were adapted with permission from Copyright (2009) Springer Nature. [197]*

4.5.3 Printability of the CNF/GGMMA inks

The printability of the formulated CNF/GGMMA inks was investigated using an INVIVO 3D printer (Korea) assisted with screw-driven printing head and dispensing tips (27 GA). The printed process was aided with a drop of 5 w/v % Ca^{2+} solution on the first layer of the printed objects. After printing, the whole geometry was cross-linked exposing to UV light for 5 min. As shown in **Figure 4.18**, the printed scaffolds, a spruce tree model, and nose model kept well their shape fidelity and high resolution. In addition, the printed scaffold represented a lightweight but strong material, which could be lifted by a spatula and even with a sharp needle. In particular, the printed objects displayed a sharp and distinct edge (**Figure 4.18b**) and inner structure (**Figure 4.18g**). These features would improve the performance of the CNF/GGMMA inks in the fabrication of objects with complex geometry and hierarchical porosity, aiming at more precisely mimicking the native tissues. [198]

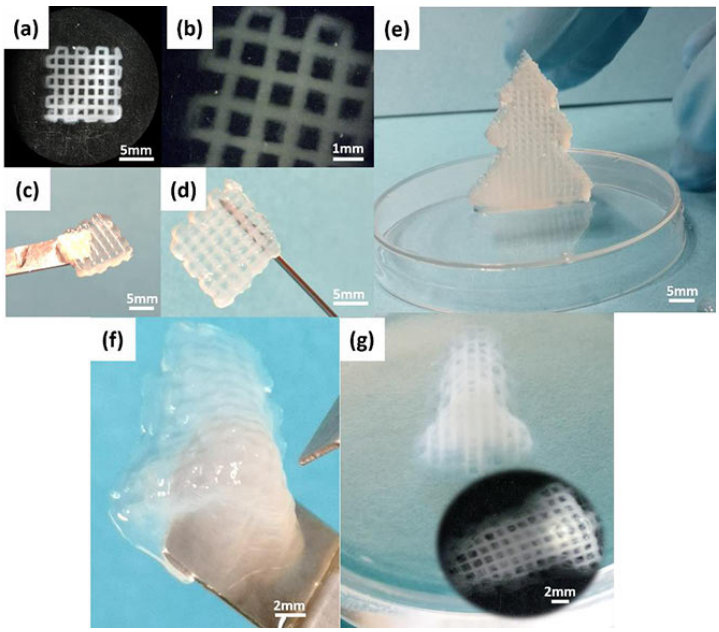

Figure 4.18. *Scaffolds with high resolution were printed with ink IA after UV cross-linking (a-d). The top view (a), edge view (b), handling with spatula (c), and holding with needle (d) of the printed scaffold with dimension of 10mm x 10mm x 2mm. (e) Standing printed and cross-linked spruce tree model with ink IIB. (f and g) Printed and cross-linked nose model with inner structure in high resolution.*

4.6 CNF-based scaffolds for cell culture

CNF-based scaffold supporting 3T3 fibroblast culture

The biocompatibility of the 3D printed scaffolds is the prerequisite for the material to be used as an ECM-mimicking matrix. In this study, a mouse 3T3 fibroblast cell line was chosen to test the feasibility of the printed CNF/GelMA scaffolds to be used for wound dressing. The incorporation of GelMA changed the properties of the printed scaffold, including cell adhesion motifs (*i.e.* RGDs), mechanical properties, topographical features, and porosity, which have to be overall considered for cell migration, viability, and proliferation. [184, 196]

The cell adhesion capability was measured using a crystal violet assay after 12 hours of cell incubation in the existence of the scaffolds. Compared with the 2D control, cell adhesion to only CNF scaffolds decreased, whereas the incorporation of GelMA improved the cell adhesion (**Figure 4.19a**). It might be due to that the GelMA with the RGD motifs promoted cell attachment. [21, 199] The cell viability against the printed scaffolds was evaluated as shown in **Figure 4.19b**. It was found that the printed CNF/GelMA scaffolds had no adverse effect on cell viability. This is consistent with our previous studies regarding the

cytotoxicity test of TEMPO-oxidized CNF that is well compatible with epithelial-derived Hela cells and hematopoietic-derived Jurkat cells. [75, 200] Meanwhile, the cell viability test suggests that the established printing procedure is a friendly one to fibroblast cell line.

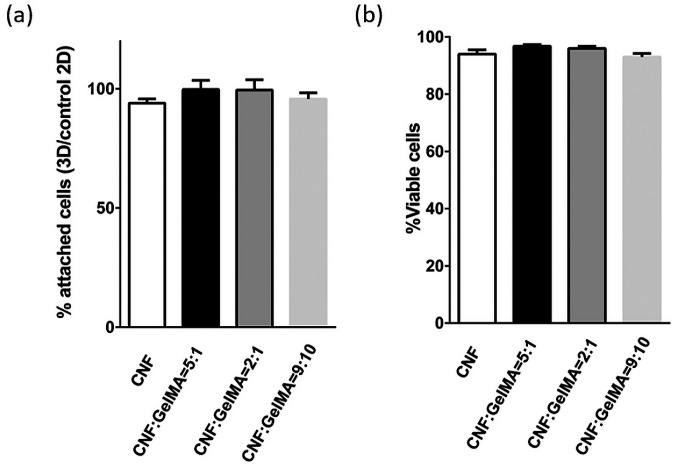

Figure 4.19. *3T3 fibroblast cells were incubated with indicated 3D matrix in a density of 1×10^5 cells /24-well. (a) The cell adhesion was measured after 12 h of incubate using crystal violet assay. (b) The cell survival rate was measured after 24 h of incubation by using MTT assay. Bar=mean ± STDEV; n=4.*

The cell proliferation on the CNF/GelMA scaffolds was evaluated in an incubation period of 72 h. As observed in **Figure 4.20**, the number of cells on the sample of CNF:GelMA=5:1 were two times higher compared to the number cells on only CNF scaffolds. However, the higher ratio of GelMA in the scaffolds (CNF:GelMA=2:1 and CNF:GelMA=10:9) had a weaker effect on promoting cell proliferation. According to a recent study, [179] the improved fibroblast cell proliferation is well correlated with the improved mechanical property of the matrix. However, the Young's modulus increased with the addition of more GelMA, whereas the cell proliferation decreased. It might be because other factors like topography of the printed struts and porosity could regulate the cell proliferation. [201, 202] In **Figure 4.9 (e, j, o, and t**), the morphology of the printed struts in the scaffolds became more porous while the content of GelMA increased. The wall-separated microspores on the strut surface of CNF:GelMA=9:10 were around 5-20 µm as measured in the sample after freeze-drying (**Figure 4.9t**). These pore dimensions are anticipated to be almost comparable to the size of mouse 3T3 fibroblast cells (50-150 µm) after swelling. It is assumed that the wall-like morphology might intervene the cell migration if the fibroblasts could likely be entrapped in the network. [203]

Based on the above studies, the importance of manipulating GelMA content when engineering such a matrix for potent fibroblast cell proliferation is

stressed and further prompt the wound dressing application. The lack of noticeable toxic effect and the promoted proliferative activity of 3T3 fibroblasts with the CNF/GelMA scaffolds offer good opportunities in wound healing therapy.

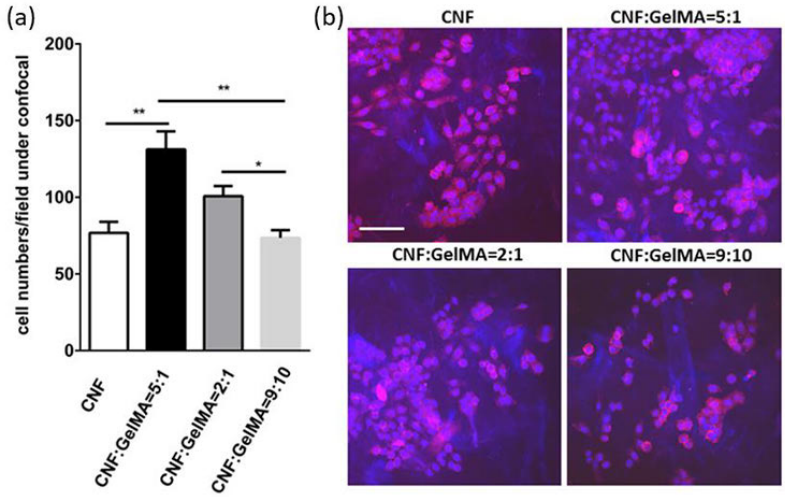

Figure 4.20. *3T3 fibroblast cells were incubated with indicated 3D matrix in a density of 1×10^5 cells/24-well. (a) The cell proliferation and (b) representative confocal images were measured after 3 days of incubation. Scale bar, 50 μm. Bar=mean ± STDEV; n=4. *, p<0.1; **, p<0.01.*

5. Conclusions and future perspectives

5.1 Highlights of this thesis

This thesis work has highlighted the comprehensive utilization of renewable wood-derived biopolymers in the development of different types of inks for 3D printing. GGM, TEMPO-oxidized CNFs, and other biopolymers, *i.e.* PLA and GelMA were utilized to facilitate versatile ink formulations. In addition, in order to enhance the shape fidelity and obtain mechanically tunable printed objects, cross-linkable GGM derivatives, *i.e.* GGMTA and GGMMA, were prepared by facile synthesis approaches and used in conjugation with nanocellulose. The printability of the prepared filaments and hydrogel inks was demonstrated with different printing techniques.

As one branch of the study, bulk GGM was successfully utilized with PLA to prepare filament materials for FDM 3D printing. A co-solvent blending approach was established for evenly mixing the two biopolymers with different polarity. The scaffolds of the PLA/GGM filaments demonstrated the potential of being used in 3D printing. Moreover, the mechanical and morphological properties of the PLA/GGM filaments and scaffolds with up to 20 wt.% GGM were comparable with that of PLA. The remarkable results obtained in this work demonstrate the potential of developing value-added products from side-stream wood-derived GGM.

As another branch of the thesis study, we demonstrated the utilization of CNF hydrogel for DIW 3D printing ink formulations. As an auxiliary material, GelMA was successfully introduced to CNF hydrogel. It was demonstrated that the CNF with negative charge facilitated the possibility of the GelMA with concentration less than 1 w/v % being cross-linked *via* UV. GelMA was assembled onto the CNFs *via* ionic interactions or hydrogen bonding, which promoted the low-concentration ink formulation. The formulation and characterization of the CNF/GelMA inks offers promising new avenues that take advantage of such inks in biofabrication.

Furthermore, two facile synthesis approaches have been developed to functionalize GGM as cross-linking precursors for the CNF-based ink formulations, inspired by the intrinsic affinity of hemicellulose to cellulose. In one approach, tyramine-conjugated GGM was synthesized by firstly introducing carboxylic groups *via* TEMPO-oxidation and then amine coupling with tyramine. In the other approach, the GGM methacrylate was efficiently prepared by reacting with methacrylic anhydride in aqueous media and controlled pH and temperature. The GGM functionalized with different degrees of substitution of the tyramine and methacrylate groups were proven to be enzymatic and UV-aided cross-linked, respectively. The rapid gelation window of the functionalized GGM prompts GGM being a promising hydrogel in

biofabrication and biomedical applications, which require tunable mechanical properties.

Based on the gelation window of the functionalized GGM, the in-house GGMMA was chosen for the biomimetic ink formulation with CNFs. It was demonstrated that the versatile CNF/GGMMA inks exhibited a wide spectrum of mechanical properties, which displays a significant potential as the platform material suitable for culturing different cell lines. The performance of CNF/GGMMA inks on the extra-high resolution and good shape fidelity of the printed geometries opens the possibilities for the precise fabrication of complex tissues or organs.

Lastly, the biocompatibility of CNF-based scaffolds was evaluated by mouse 3T3 fibroblast cell viability and proliferation. The low-concentration inks were demonstrated to fabricate bioactive scaffolds with tunable mechanical performance and controllable topography. The formulated versatile inks and established mild fabrication method indicated a promising methodology in biomedical applications such as wound healing.

Overall, this thesis work underlines the urge to innovative research in the field of 3D printing of wood-based biopolymers especially towards biomedical applications. The interdisciplinary knowledge regarding wood-derived materials, 3D printing, and biomedical applications are established for further study. The high potential for the highly value-added plant-based materials is exhibited within the scope of bioeconomy.

5.2 Future perspectives

It is undoubtable that wood-derived biopolymers are promising candidates as biomaterial substrates in biomedical applications. Nanocellulose with its outstanding properties such as biocompatibility, outstanding mechanical properties, mimicking the ECM tissues, and *in vitro* biodegradability is currently extensively employed as a new generation of nanomaterials for biomedical applications. However, the application of nanocellulose and hemicelluloses still faces numerous challenges to meet the application requirements. Firstly, the *in vivo* biodegradability of nanocellulose and hemicelluloses is one of the most critical concerns considering their use as the implant materials. Moreover, the preparation process of nanocellulose is yet neither economically feasible nor environmentally friendly. To certain extent, the cost of the medical grade nanocellulose products is another hindrance to the related comprehensive studies and further in-depth work in the development of applications. Moreover, the wood-derived biopolymers are so-called bio-inert materials, which are providing excellent biocompatibility without promoting biological activities. Thus, certain applicable and nontoxic functionalization is required to bring bioactivity to wood biopolymers, which could boost the application of wood-derived biopolymer in the field of tissue engineering.

Nevertheless, other interdisciplinary studies combining specific drug-delivery would offer better solutions in the regard of potential biomedical or pharmaceutical applications. Last but not the least, regarding 3D bioprinting of wood-derived biopolymers, compressive and extensive studies on the simulation of the printing process with cells will bring us better images to understand *in vivo* tissue mimics.

6. Acknowledgements

This doctoral thesis was carried out during the time of 07.2015-12.2018 in the laboratory of Wood and Paper Chemistry at the Faculty of Science and Engineering of Åbo Akademi University. This work received the main funding from the Johan Gadolin Process Chemistry Centre of Åbo Akademi University. The travel grants from Harry Elvings legat and research grants from Finnish Paper Engineers' Association, as well as funding from Australian ARC Centre of Excellence for Electromaterials Science (CE140100012) during the stay in the University of Wollongong are mostly acknowledged.

I would like to express my deepest gratitude to Professor Stefan Willför and Adjunct Professor Chunlin Xu, for their supervision and endless support! THANK YOU! Big thanks to Prof. Willför who offered me this great opportunity meanwhile supplied rich freedom, facilities, and opportunities. I felt even a bit 'stressful' to see such many new 3D printers coming to our lab during my study years. However, that is really one of the driven-forces for my graduation☺. Adjunct Professor Xu, is such supervisor who also stand behind you whenever you are going to find him for help. It seems like he has his email set as 'auto-reply' with different answers regarding to different questions. I also want to thank him always giving answers with 'non-absolute answers' to my questions, which actually guided me to the right answers and tell me HOW to cope with difficulties for the researches and life. A big thank goes to Academy lecturer, Docent Anna Sundberg who helped me with proof reading my thesis at the speed of light. To voluntarily read this tome within three days is quite impressive! She was also my supervisor with my master thesis. She always keep her rigorous attitude to academic works and language even for a 'period'. She has also offered me many opportunities to practice my language, my supervision skills and taught me how to be a team worker. Dr. Xiaoju Wang, a co-supervisor, came to my last stage of PhD studies. As her multidisciplinary background, she really is a knowledge database broadening my concepts and sights. Nevertheless, she has really showed a model for me how to be an effective writer! I felt such lucky and happy to have you for discussing any type of questions.

The gratitude goes to Professor Gordon G. Wallace for offering me the opportunity to visit the Intelligent Polymer Research Institute (IPRI), ARC Centre of Excellence for Electromaterials Science, University of Wollongong, Australia. The time in Australia broadened my sights and views and was very helpful to my research career. All the colleagues at IPRI, especially Dr. Binbin Zhang Molino, Dr. Zhilian Yue, Dr. Paul J. Molino, Mr. Yuchao Fan, Mr. Jianfeng Li, Miss. Guyue Bo, etc are acknowledged for your all kinds of supports with research and life. Professor Thomas Rosenau, Professor Antje Potthast, Dr. Hassan Mohamed Amer, and Dr. Markus Bacher in the University of Nature Resources and Life Sciences (BOKU), Austria, are especially thanked for giving me a chance to visit and deeply learn running different NMR techniques. A special thank goes to Professor Jun Liu at Jiangsu University and

Professor Bin Li at Qingdao Institute of Bioenergy and Bioprocess Technology, Chinese Academy of Science. You two are deeply wise and trusted adviser and helper to me. No mentors work better than you two do. I also want to thank the teachers and friends in Qilu University of Technology (Jinan, China) for all the great memorable time and endless support. Special thanks to all the teachers in the school of light chemical engineering, especially Professor Chuanshan Zhao who has strongly encouraged me to purse my degrees oversea.

I also would like to thank all the collaborators, especially, Dr. Kajsa Markstedt, Mr. Peter Uppstu, Dr. Otto Långvik, Dr. Dennis Kronlund, Ms. Heidi Öblom, Dr. Niko Moritz, Dr. Maren Preis, Ms. Peiru Yang, Prof. Fang Cheng, Prof. Paul Gatenholm, Prof. Monika Österberg, and Prof. Niklas Sandler. We could not have all the nice works without all your contributions.

All the current and former colleagues at the Laboratory of Wood and Paper Chemistry. Especially, Andrey with his stories and enthusiastic passion to academic works always inspired me. Jalle is always ready to offer solutions whenever and wherever I came cross the experimental or technical issues. Annika with her skillful GS-MS helped me out of many molecule identification questions! Other friends in 3PK like Basti, Lari, Anders, Katja, Matias, Yongchao, Weihua, Huanfei, Qingbo, and Luyao are mostly acknowledged for the talks, scientific discussions, laughs, and all great times spent together.

All my Chinese friends in Turku, and Helsinki area of Finland, thank you all for your enthusiastic help and all the wonderful time together. You brought me with lots of colorful spare time with interesting activities and homemade tasty foods.☺ We are forever the family!

Last but not least, I would like to express my deepest gratitude to my loving family and the relatives for their endless love, support, and encouragement. I also want to express my gratitude to my two elder-brothers, Mr. Jiang Wang and Dr. Jinfeng Ding, and sister-in-law, Mrs. Chunling Wang. You are the models for my life! My dear parents, parents-in-law, sister, brother-in-law, and my beloved wife and the little boy, thank you all! I love you all!

7. References

1. Alberts, B., Johnson, A., Lewis, J., Walter, P., Raff, M. and Roberts, K., 2002. Molecular Biology of the Cell 4th Edition: International Student Edition.
2. Gefen, A. ed., 2009. Studies in Mechanobiology, Tissue Engineering and Biomaterials. Springer.
3. Theocharis, A.D., Skandalis, S.S., Gialeli, C. and Karamanos, N.K., 2016. Extracellular matrix structure. *Advanced drug delivery reviews*, **97**, 4-27.
4. Cukierman, E., Pankov, R. and Yamada, K.M., 2002. Cell interactions with three-dimensional matrices. *Current opinion in cell biology*, **14**(5),633-640.
5. Ratner, B.D., Hoffman, A.S., Schoen, F.J. and Lemons, J.E., 2006. Biomaterials science: an introduction to materials in medicine. *MRS Bull*, **31**, 59.
6. Yang, S., Leong, K.F., Du, Z. and Chua, C.K., 2001. The design of scaffolds for use in tissue engineering. Part I. Traditional factors. *Tissue engineering*, **7**(6), 679-689.
7. Badylak, S.F., Freytes, D.O. and Gilbert, T.W., 2009. Extracellular matrix as a biological scaffold material: structure and function. *Acta biomaterialia*, **5**(1), 1-13.
8. Seliktar, D., 2012. Designing cell-compatible hydrogels for biomedical applications. *Science*, **336**(6085), 1124-1128.
9. Freyman, T.M., Yannas, I.V. and Gibson, L.J., 2001. Cellular materials as porous scaffolds for tissue engineering. *Progress in Materials science*, **46**(3-4), 273-282.
10. Posnett, J. and Franks, P.J., 2007. Skin Breakdown, The Silent Epidemic. *London, UK: Smith and Nephew.*
11. Lindholm, C. and Searle, R., 2016. Wound management for the 21st century: combining effectiveness and efficiency. *International wound journal*, **13**, 5-15.
12. Eucomed Wound Care Policy Paper. http://ewma.org/fileadmin/user_upload/EWMA/pdf/EWMA_Projects/090923__Wound_Care_Brochure_final.pdf [accessed on August 2018].
13. Bhardwaj, N., Chouhan, D. and B Mandal, B., 2017. Tissue engineered skin and wound healing: current strategies and future directions. *Current pharmaceutical design,* **23**(24), 3455-3482.
14. Posnett, J., Gottrup, F., Lundgren, H. and Saal, G., 2009. The resource impact of wounds on health-care providers in Europe. *Journal of wound care*, **18**(4), 154-154.
15. Burg, K.J., Porter, S. and Kellam, J.F., 2000. Biomaterial developments for bone tissue engineering. *Biomaterials*, **21**(23), 2347-2359.
16. Ko, H.F., Sfeir, C. and Kumta, P.N., 2010. Novel synthesis strategies for natural polymer and composite biomaterials as potential scaffolds for tissue engineering. Philosophical Transactions of the Royal Society of London A: Mathematical, *Physical and Engineering Sciences*, **368**(1917), 1981-1997.
17. O'brien, F.J., 2011. Biomaterials & scaffolds for tissue engineering. *Materials today*, **14**(3), 88-95.
18. Wang, J.Y., Wang, K., Gu, X. and Luo, Y., 2016. Polymerization of hydrogel network on microfiber surface: synthesis of hybrid water-absorbing matrices for biomedical applications. *ACS Biomaterials Science & Engineering*, **2**(6), 887-892.
19. Kim, B.S., Baez, C.E. and Atala, A., 2000. Biomaterials for tissue engineering.

World journal of urology, **18**(1), 2-9.

20. Hoffman, A.S., 2012. Hydrogels for biomedical applications. *Advanced drug delivery reviews*, **64**, 18-23.
21. Yue, K., Trujillo-de Santiago, G., Alvarez, M.M., Tamayol, A., Annabi, N. and Khademhosseini, A., 2015. Synthesis, properties, and biomedical applications of gelatin methacryloyl (GelMA) hydrogels. *Biomaterials*, **73**, 254-271.
22. Lanza, R., Langer, R. and Vacanti, J.P. eds., 2011. Principles of tissue engineering. Academic press.
23. Dash, M., Chiellini, F., Ottenbrite, R.M. and Chiellini, E., 2011. Chitosan—A versatile semi-synthetic polymer in biomedical applications. *Progress in polymer science*, **36**(8), 981-1014.
24. Lee, K.Y. and Mooney, D.J., 2012. Alginate: properties and biomedical applications. *Progress in polymer science*, **37**(1), 106-126.
25. Gatenholm, P., Martinez, H., Karabulut, E., Amoroso, M., Kölby, L., Markstedt, K., Gatenholm, E. and Henriksson, I., 2018. Development of nanocellulose-based bioinks for 3d bioprinting of soft tissue. *3D Printing and Biofabrication,* 331-352.
26. Syverud, K., 2017. Tissue Engineering Using Plant-Derived Cellulose Nanofibrils (CNF) as Scaffold Material, in Nanocelluloses: Their Preparation, Properties, and Applications. *American Chemical Society*, 171-189.
27. http://www.int.laborundmore.com/archive/543411/Development-of-the-next-generation-of-synthetic-extracellular-matrices-for-3D-cell-culture.html, [accessed on August 2018].
28. Lin, N. and Dufresne, A., 2014. Nanocellulose in biomedicine: Current status and future prospect. *European Polymer Journal*, **59**, 302-325.
29. Kalia, S., Dufresne, A., Cherian, B.M., Kaith, B.S., Avérous, L., Njuguna, J. and Nassiopoulos, E., 2011. Cellulose-based bio-and nanocomposites: a review. *International Journal of Polymer Science*, **2011**.
30. Moon, R.J., Martini, A., Nairn, J., Simonsen, J. and Youngblood, J., 2011. Cellulose nanomaterials review: structure, properties and nanocomposites. *Chemical Society Reviews*, **40**(7), 3941-3994.
31. Zhu, H., Luo, W., Ciesielski, P.N., Fang, Z., Zhu, J.Y., Henriksson, G., Himmel, M.E. and Hu, L., 2016. Wood-derived materials for green electronics, biological devices, and energy applications. *Chemical Reviews*, **116**(16), 9305-9374.
32. Côté, W.A. and Syracuse University (New York). Advanced Science Seminar (1964: Upper Saranac Lake NY), 1965. Cellular ultrastructure of woody plants: proceedings of the Advanced Science Seminar, Pinebrook Conference Center, Upper Saranac Lake, New York, September, 1964. *Syracuse University Press*.
33. Postek, M.T., Vladár, A., Dagata, J., Farkas, N., Ming, B., Wagner, R., Raman, A., Moon, R.J., Sabo, R., Wegner, T.H. and Beecher, J., 2010. Development of the metrology and imaging of cellulose nanocrystals. *Measurement Science and Technology*, **22**(2), 024005.
34. Klemm, D., Heublein, B., Fink, H.P. and Bohn, A., 2005. Cellulose: fascinating biopolymer and sustainable raw material. *Angewandte Chemie International Edition*, **44**(22), 3358-3393.
35. Hoffmann, P. and M. Jones, 1990. Structure and degradation process for waterlogged archaeological wood. *Advances in Chemistry,* **225**, 35-65.

36. Lewin, M. and Goldstein, I.S., 1991. Wood Structure and Composition. CRC Press.
37. Klemm, D., Philpp, B., Heinze, T., Heinze, U. and Wagenknecht, W., 1998. Comprehensive cellulose chemistry. Volume 1: Fundamentals and analytical methods. Wiley-VCH Verlag GmbH.
38. Li, Q. and Renneckar, S., 2011. Supramolecular structure characterization of molecularly thin cellulose I nanoparticles. *Biomacromolecules*, **12**(3), 650-659.
39. Sjostrom, E., 2013. Wood chemistry: fundamentals and applications. Elsevier.
40. Fengel, D. and Wegener, G., 1983. Wood: Chemistry, Ultrastructure, Reactions. Walter de Gruyter.
41. Sixta, H., Süss, H.U., Potthast, A., Schwanninger, M. and Krotscheck, A.W., 2006. Pulp Bleaching: Sections 7.1–7.3. 5. *Handbook of pulp*, 609-708.
42. Peniche, C., Argüelles-Monal, W. and Goycoolea, F.M., 2008. Monomers, polymers and composites from renewable resources. *Amsterdam: Elsevier,* 517-542.
43. Lionetti, V., Giancaspro, A., Fabri, E., Giove, S.L., Reem, N., Zabotina, O.A., Blanco, A., Gadaleta, A. and Bellincampi, D., 2015. Cell wall traits as potential resources to improve resistance of durum wheat against Fusarium graminearum. *BMC plant biology*, **15**(1), 6.
44. Verma, S.R. and Dwivedi, U.N., 2014. Lignin genetic engineering for improvement of wood quality: Applications in paper and textile industries, fodder and bioenergy production. *South African Journal of Botany,* **91**, 107-125.
45. Tsoumis, G., 1991. Science and technology of wood: structure, properties, utilization. Vol. 115. Van Nostrand Reinhold New York.
46. Klemm, D., Kramer, F., Moritz, S., Lindström, T., Ankerfors, M., Gray, D. and Dorris, A., 2011. Nanocelluloses: a new family of nature‐based materials. *Angewandte Chemie International Edition*, **50**(24), 5438-5466.
47. Esa, F., Tasirin, S.M., and Rahman, N.A., 2014. Overview of bacterial cellulose production and application. *Agriculture and Agricultural Science Procedia*, **2**, 113-119.
48. Börjesson, M. and G. Westman, 2015. Crystalline nanocellulose—preparation, modification, and properties, in Cellulose—Fundamental Aspects and Current Trends. InTech.
49. Brown, A.J., 1886. XLIII.—On an acetic ferment which forms cellulose. Journal of the Chemical Society, Transactions, **49**, 432-439.
50. Hestrin, S. and Schramm, M., 1954. Synthesis of cellulose by Acetobacter xylinum. 2. Preparation of freeze-dried cells capable of polymerizing glucose to cellulose. *Biochemical Journal*, **58**(2), 345.
51. Stanisławska, A., 2016. Bacterial nanocellulose as a microbiological derived nanomaterial. *Advances in Materials Science*, **16**(4), 45-57.
52. Andrade, F., Pertile, R., Dourado, F. and Gama, F.M., 2010. Bacterial cellulose: properties, production and applications.
53. Guhados, G., Wan, W., and Hutter, J.L., 2005. Measurement of the elastic modulus of single bacterial cellulose fibers using atomic force microscopy. *Langmuir*, **21**(14), 6642-6646.
54. Hsieh, Y.C., Yano, H., Nogi, M. and Eichhorn, S.J., 2008. An estimation of the Young's modulus of bacterial cellulose filaments. *Cellulose*, **15**(4), 507-513.

55. Svensson, A., Nicklasson, E., Harrah, T., Panilaitis, B., Kaplan, D.L., Brittberg, M. and Gatenholm, P., 2005. Bacterial cellulose as a potential scaffold for tissue engineering of cartilage. *Biomaterials*, **26**(4), 419-431.
56. Bielecki, S., Kalinowska, H., Krystynowicz, A., Kubiak, K., Kołodziejczyk, M. and De Groeve, M., 2012. Wound dressings and cosmetic materials from bacterial nanocellulose. *Bacterial Nanocellulose: A Sophisticated Multifunctional Material. Perspectives in Nanotechnology*.
57. Klemm, D., Schumann, D., Udhardt, U. and Marsch, S., 2001. Bacterial synthesized cellulose—artificial blood vessels for microsurgery. *Progress in polymer science*, **26**(9), 1561-1603.
58. Schumann, D.A., Wippermann, J., Klemm, D.O., Kramer, F., Koth, D., Kosmehl, H., Wahlers, T. and Salehi-Gelani, S., 2009. Artificial vascular implants from bacterial cellulose: preliminary results of small arterial substitutes. *Cellulose*, **16**(5), 877-885.
59. Ougiya, H., Watanabe, K., Morinaga, Y. and Yoshinaga, F., 1997. Emulsion-stabilizing effect of bacterial cellulose. *Bioscience, biotechnology, and biochemistry*, **61**(9), 1541-1545.
60. Chawla, P.R., Bajaj, I.B., Survase, S.A. and Singhal, R.S., 2009. Microbial cellulose: fermentative production and applications. *Food Technology & Biotechnology*, **47**(2).
61. Martins, I.M., Magina, S.P., Oliveira, L., Freire, C.S., Silvestre, A.J., Neto, C.P. and Gandini, A., 2009. New biocomposites based on thermoplastic starch and bacterial cellulose. *Composites Science and Technology*, **69**(13), 2163-2168.
62. Jozala, A.F., de Lencastre-Novaes, L.C., Lopes, A.M., de Carvalho Santos-Ebinuma, V., Mazzola, P.G., Pessoa-Jr, A., Grotto, D., Gerenutti, M. and Chaud, M.V., 2016. Bacterial nanocellulose production and application: a 10-year overview. *Applied microbiology and biotechnology*, **100**(5), 2063-2072.
63. Herrick, F.W., Casebier, R.L., Hamilton, J.K. and Sandberg, K.R., 1983. Microfibrillated cellulose: morphology and accessibility. *Joural of Applied Polymer Science: Applied Polymer Symposium*, **37**, 9.
64. Turbak, A.F., Snyder, F.W., and Sandberg, K.R., 1983. Microfibrillated cellulose, a new cellulose product: properties, uses, and commercial potential. *Joural of Applied Polymer Science: Applied Polymer Symposium*, **37**, 8.
65. Henriksson, M., Henriksson, G., Berglund, L.A. and Lindström, T., 2007. An environmentally friendly method for enzyme-assisted preparation of microfibrillated cellulose (MFC) nanofibers. *European Polymer Journal*, **43**(8), 3434-3441.
66. Saito, T. and Isogai, A., 2004. TEMPO-mediated oxidation of native cellulose. The effect of oxidation conditions on chemical and crystal structures of the water-insoluble fractions. Biomacromolecules, **5**(5), 1983-1989.
67. Wågberg, L., Decher, G., Norgren, M., Lindström, T., Ankerfors, M. and Axnäs, K., 2008. The build-up of polyelectrolyte multilayers of microfibrillated cellulose and cationic polyelectrolytes. *Langmuir*, **24**(3), 784-795.
68. Sehaqui, H., Mautner, A., de Larraya, U.P., Pfenninger, N., Tingaut, P. and Zimmermann, T., 2016. Cationic cellulose nanofibers from waste pulp residues and their nitrate, fluoride, sulphate and phosphate adsorption properties. *Carbohydrate polymers*, **135**, 334-340.

69. Hauser, P.J. and Tabba, A.H., 2002. Dyeing Cationic Cotton with Fiber Reactive Dyes: Effect of Reactive Chemistries. *AATCC review*, **2**(5), 36-39.
70. Fan, M. and Fu, F., 2016. Advanced high strength natural fibre composites in construction. Woodhead Publishing.
71. Iwamoto, S., Kai, W., Isogai, T., Saito, T., Isogai, A. and Iwata, T., 2010. Comparison study of TEMPO-analogous compounds on oxidation efficiency of wood cellulose for preparation of cellulose nanofibrils. *Polymer Degradation and Stability*, **95**(8), 1394-1398.
72. Alexandrescu, L., Syverud, K., Gatti, A. and Chinga-Carrasco, G., 2013. Cytotoxicity tests of cellulose nanofibril-based structures. *Cellulose*, **20**(4), 1765-1775.
73. Nechyporchuk, O., Belgacem, M.N., and Pignon F., 2016. Current progress in rheology of cellulose nanofibril suspensions. *Biomacromolecules*, **17**(7), 2311-2320.
74. Vartiainen, J., Pöhler, T., Sirola, K., Pylkkänen, L., Alenius, H., Hokkinen, J., Tapper, U., Lahtinen, P., Kapanen, A., Putkisto, K. and Hiekkataipale, P., 2011. Health and environmental safety aspects of friction grinding and spray drying of microfibrillated cellulose. *Cellulose*, **18**(3), 775-786.
75. Liu, J., Chinga-Carrasco, G., Cheng, F., Xu, W., Willför, S., Syverud, K. and Xu, C., 2016. Hemicellulose-reinforced nanocellulose hydrogels for wound healing application. *Cellulose*, **23**(5), 3129-3143.
76. Lou, Y.R., Kanninen, L., Kuisma, T., Niklander, J., Noon, L.A., Burks, D., Urtti, A. and Yliperttula, M., 2013. The use of nanofibrillar cellulose hydrogel as a flexible three-dimensional model to culture human pluripotent stem cells. *Stem cells and development*, **23**(4), 380-392.
77. Markstedt, K., Mantas, A., Tournier, I., Martínez Ávila, H., Hägg, D. and Gatenholm, P., 2015. 3D bioprinting human chondrocytes with nanocellulose–alginate bioink for cartilage tissue engineering applications. *Biomacromolecules*, **16**(5), 1489-1496.
78. Nickerson, R.F. and Habrle, J.A., 1947. Cellulose intercrystalline structure. *Industrial & Engineering Chemistry*, **39**(11), 1507-1512.
79. Frey-Wyssling, A., 1954. The fine structure of cellulose microfibrils. *Science*, **119**(3081), 80-82.
80. Yu, H., Qin, Z., Liang, B., Liu, N., Zhou, Z. and Chen, L., 2013. Facile extraction of thermally stable cellulose nanocrystals with a high yield of 93% through hydrochloric acid hydrolysis under hydrothermal conditions. *Journal of Materials Chemistry A*, **1**(12), 3938-3944.
81. Camarero Espinosa, S., Kuhnt, T., Foster, E.J. and Weder, C., 2013. Isolation of thermally stable cellulose nanocrystals by phosphoric acid hydrolysis. *Biomacromolecules*, **14**(4), 1223-1230.
82. Cao, Y., Jiang, Y., Song, Y., Cao, S., Miao, M., Feng, X., Fang, J. and Shi, L., 2015. Combined bleaching and hydrolysis for isolation of cellulose nanofibrils from waste sackcloth. *Carbohydrate polymers*, **131**, 152-158.
83. Liu, Y., Wang, H., Yu, G., Yu, Q., Li, B. and Mu, X., 2014. A novel approach for the preparation of nanocrystalline cellulose by using phosphotungstic acid. *Carbohydrate polymers*, **110**, 415-422.
84. Li, B., Xu, W., Kronlund, D., Määttänen, A., Liu, J., Smått, J.H., Peltonen, J.,

Willför, S., Mu, X. and Xu, C., 2015. Cellulose nanocrystals prepared via formic acid hydrolysis followed by TEMPO-mediated oxidation. *Carbohydrate polymers*, **133**, 605-612.

85. Xu, W., Grénman, H., Liu, J., Kronlund, D., Li, B., Backman, P., Peltonen, J., Willför, S., Sundberg, A. and Xu, C., 2017. Mild Oxalic-Acid-Catalyzed Hydrolysis as a Novel Approach to Prepare Cellulose Nanocrystals. *ChemNanoMat*, **3**(2), 109-119.
86. Chen, L., Zhu, J.Y., Baez, C., Kitin, P. and Elder, T., 2016. Highly thermal-stable and functional cellulose nanocrystals and nanofibrils produced using fully recyclable organic acids. *Green Chemistry*, **18**(13), 3835-3843.
87. Hirota, M., Tamura, N., Saito, T. and Isogai, A., 2009. Oxidation of regenerated cellulose with NaClO2 catalyzed by TEMPO and NaClO under acid-neutral conditions. *Carbohydrate polymers*, **78**(2), 330-335.
88. Montanari, S., Roumani, M., Heux, L. and Vignon, M.R., 2005. Topochemistry of carboxylated cellulose nanocrystals resulting from TEMPO-mediated oxidation. *Macromolecules*, **38**(5), 1665-1671.
89. Satyamurthy, P., Jain, P., Balasubramanya, R.H. and Vigneshwaran, N., 2011. Preparation and characterization of cellulose nanowhiskers from cotton fibres by controlled microbial hydrolysis. *Carbohydrate Polymers*, **83**(1), 122-129.
90. Filson, P.B., Dawson-Andoh, B.E., and Schwegler-Berry, D., 2009. Enzymatic-mediated production of cellulose nanocrystals from recycled pulp. *Green Chemistry*, **11**(11), 1808-1814.
91. Tang, L.R., Huang, B., Ou, W., Chen, X.R. and Chen, Y.D., 2011. Manufacture of cellulose nanocrystals by cation exchange resin-catalyzed hydrolysis of cellulose. *Bioresource Technology*, **102**(23), 10973-10977.
92. Beck-Candanedo, S., Roman, M., and Gray, D.G., 2005. Effect of reaction conditions on the properties and behavior of wood cellulose nanocrystal suspensions. *Biomacromolecules*, **6**(2), 1048-1054.
93. Rahimi, M. and Behrooz, R., 2011. Effect of cellulose characteristic and hydrolyze conditions on morphology and size of nanocrystal cellulose extracted from wheat straw. *International Journal of Polymeric Materials*, **60**(8), 529-541.
94. Brito, B.S., Pereira, F.V., Putaux, J.L. and Jean, B., 2012. Preparation, morphology and structure of cellulose nanocrystals from bamboo fibers. *Cellulose*, **19**(5), 1527-1536.
95. Berg, van den O., Capadona, J.R., and Weder, C., 2007. Preparation of homogeneous dispersions of tunicate cellulose whiskers in organic solvents. *Biomacromolecules*, **8**(4), 1353-1357.
96. Šturcová, A., G.R. Davies, and S.J. Eichhorn, 2005. Elastic modulus and stress-transfer properties of tunicate cellulose whiskers. *Biomacromolecules*, **6**(2), 1055-1061.
97. Wang, Q., Du, H., Zhang, F., Zhang, Y., Wu, M., Yu, G., Liu, C., Li, B. and Peng, H., 2018. Flexible cellulose nanopaper with high wet tensile strength, high toughness and tunable ultraviolet blocking ability fabricated from tobacco stalk via a sustainable method. *Journal of Materials Chemistry A*, **6**, 13021-13030
98. Habibi, Y., Lucia, L.A., and Rojas, O.J., 2010. Cellulose nanocrystals: chemistry, self-assembly, and applications. *Chemical Reviews*, **110**(6), 3479-3500.
99. Chen, L., Wang, Q., Hirth, K., Baez, C., Agarwal, U.P. and Zhu, J.Y., 2015. Tailoring

the yield and characteristics of wood cellulose nanocrystals (CNC) using concentrated acid hydrolysis. *Cellulose*, **22**(3), 1753-1762.
100. Nishino, T., Matsuda, I., and Hirao, K., 2004. All-cellulose composite. *Macromolecules*, **37**(20), 7683-7687.
101. Marchessault, R., Morehead, F., and Walter, N., 1959. Liquid crystal systems from fibrillar polysaccharides. *Nature*, **184**(4686), 632-633.
102. Revol, J.-F., Godbout, L., and Gray, D., 1998. Solid self-assembled films of cellulose with chiral nematic order and optically variable properties. *Journal of Pulp and Paper Science*, **24**(5), 146-149.
103. Gray, D.G., and Mu, X., 2015. Chiral nematic structure of cellulose nanocrystal suspensions and films; polarized light and atomic force microscopy. *Materials*, **8**(11), 7873-7888.
104. Gray, D.G., 2014. Recent advances in chiral nematic structure and iridescent color of cellulose nanocrystal films. *Nanomaterials*, **6**(11), 213.
105. Silvério, H.A., Neto, W.P.F., Dantas, N.O. and Pasquini, D., 2013. Extraction and characterization of cellulose nanocrystals from corncob for application as reinforcing agent in nanocomposites. *Industrial Crops and Products*, **44**, 427-436
106. Tang, J., Shi, Z., Berry, R.M. and Tam, K.C., 2015. Mussel-inspired green metallization of silver nanoparticles on cellulose nanocrystals and their enhanced catalytic reduction of 4-nitrophenol in the presence of β-cyclodextrin. *Industrial & Engineering Chemistry Research*, **54**(13), 3299-3308.
107. Kan, K.H., Li, J., Wijesekera, K. and Cranston, E.D., 2013. Polymer-grafted cellulose nanocrystals as pH-responsive reversible flocculants. *Biomacromolecules*, **14**(9), 3130-3139.
108. Zoppe, J.O., Venditti, R.A., and Rojas, O.J., 2012. Pickering emulsions stabilized by cellulose nanocrystals grafted with thermo-responsive polymer brushes. *Journal of Colloid and Interface Science*, **369**(1), 202-209.
109. Dong, S. and Roman, M., 2007. Fluorescently labeled cellulose nanocrystals for bioimaging applications. *Journal of the American Chemical Society*, **129**(45), 13810-13811.
110. Drogat, N., Granet, R., Sol, V., Memmi, A., Saad, N., Koerkamp, C.K., Bressollier, P. and Krausz, P., 2011. Antimicrobial silver nanoparticles generated on cellulose nanocrystals. *Journal of Nanoparticle Research*, **13**(4), 1557-1562.
111. Jorfi, M. and Foster, E.J., 2015. Recent advances in nanocellulose for biomedical applications. *Journal of Applied Polymer Science*, **132**(14), 41719
112. Barsett, H., Ebringerová, A., Harding, S.E., Heinze, T., Hromádková, Z., Muzzarelli, C., Muzzraelli, R.A.A., Paulsen, B.S. and ElSEOUD, O.A., 2005. Polysaccharides I: Structure, characterisation and use (Vol. 186). Springer Science & Business Media.
113. Popa, V., 2011. Polysaccharides in Medicinal and Pharmaceutical Applications. Smithers Rapra.
114. Sun, R., Sun, X., and Tomkinson, I., 2004. Hemicelluloses and Their Derivatives. Hemicelluloses: Science and Technology, **864**, 2-22.
115. Liu, J., Willför, S., and Xu, C., 2015. A review of bioactive plant polysaccharides: Biological activities, functionalization, and biomedical applications. *Bioactive Carbohydrates and Dietary Fibre*, **5**(1), 31-61.

116. Xu, C., Spadiut, O., Araújo, A.C., Nakhai, A. and Brumer, H., 2012. Chemo-enzymatic assembly of clickable cellulose surfaces via multivalent polysaccharides. *ChemSusChem*, **5**(4), 661-665.
117. Dax, D., Chávez, M.S., Xu, C., Willför, S., Mendonça, R.T. and Sánchez, J., 2014. Cationic hemicellulose-based hydrogels for arsenic and chromium removal from aqueous solutions. *Carbohydrate polymers*, **111**, 797-805.
118. Peng, X., Ren, J., Zhong, L., Sun, R., Shi, W. and Hu, B., 2012. Glycidyl methacrylate derivatized xylan-rich hemicelluloses: synthesis and characterizations. *Cellulose*, **19**(4), 1361-1372.
119. Kuzmenko, V., Hägg, D., Toriz, G. and Gatenholm, P., 2014. In situ forming spruce xylan-based hydrogel for cell immobilization. *Carbohydrate polymers*, **102**, 862-868.
120. Markstedt, K., Xu, W., Liu, J., Xu, C. and Gatenholm, P., 2017. Synthesis of tunable hydrogels based on O-acetyl-galactoglucomannans from spruce. *Carbohydrate polymers*, **157**, 1349-1357.
121. Maleki, L., Edlund, U., and Albertsson, A.-C., Thiolated hemicellulose as a versatile platform for one-pot click-type hydrogel synthesis. Biomacromolecules, 2015. **16**(2), 667-674.
122. Willför, S., Rehn, P., Sundberg, A., Sundberg, K. and Holmbom, B., 2003. Recovery of water-soluble acetylgalactoglucomannans from mechanical pulp of spruce. *Tappi Journal*, **2**(11), pp.27-32.
123. Song, T., Pranovich, A., Sumerskiy, I. and Holmbom, B., 2008. Extraction of galactoglucomannan from spruce wood with pressurised hot water. *Holzforschung*, **62**(6), 659-666.
124. Willför, S., Sjöholm, R., Laine, C., Roslund, M., Hemming, J. and Holmbom, B., 2003. Characterisation of water-soluble galactoglucomannans from Norway spruce wood and thermomechanical pulp. *Carbohydrate Polymers*, **52**(2), 175-187.
125. Willför, S., Sundberg, K., Tenkanen, M. and Holmbom, B., 2008. Spruce-derived mannans–A potential raw material for hydrocolloids and novel advanced natural materials. *Carbohydrate Polymers*, **72**(2), 197-210.
126. Gross, B.C., Erkal, J.L., Lockwood, S.Y., Chen, C. and Spence, D.M., 2014. Evaluation of 3D printing and its potential impact on biotechnology and the chemical sciences. *Analytical Chemistry*, **86**(7), 3240–3253.
127. Wijk, V. A. and Wijk, V. I., 2015. 3D printing with biomaterials: Towards a Sustainable and Circular Economy. IOS press.
128. Bandyopadhyay, A., Bose S., and Das S., 2015. 3D printing of biomaterials. *MRS Bulletin,* **40**(2), 108-115.
129. Murphy, S.V. and A. Atala, 2014. 3D bioprinting of tissues and organs. Nature *Biotechnology*, **32**(8), 773.
130. Melocchi, A., Parietti, F., Loreti, G., Maroni, A., Gazzaniga, A. and Zema, L., 2015. 3D printing by fused deposition modeling (FDM) of a swellable/erodible capsular device for oral pulsatile release of drugs. *Journal of Drug Delivery Science and Technology*, **30**, 360-367.
131. Chia, H.N. and Wu, B.M., 2015. Recent advances in 3D printing of biomaterials. *Journal of Biological Engineering*, **9**(1), 4.
132. Lewis, J.A., Smay, J.E., Stuecker, J. and Cesarano, J., 2006. Direct ink writing of

three‐dimensional ceramic structures. *Journal of the American Ceramic Society*, **89**(12), 3599-3609.
133. Lewis, J.A., 2006. Direct ink writing of 3D functional materials. *Advanced Functional Materials*, **16**(17), 2193-2204.
134. Xu, W., Wang, X., Sandler, N., Willför, S. and Xu, C., 2018. Three-dimensional printing of wood-derived biopolymers: A review focused on biomedical applications. *ACS sustainable chemistry & engineering*, **6**(5), 5663-5680.
135. Melnikova, R., Ehrmann, A., and Finsterbusch, K., 2014. 3D printing of textile-based structures by Fused Deposition Modelling (FDM) with different polymer materials. in IOP Conference Series: Materials Science and Engineering. IOP Publishing.
136. Sandler, N., Salmela, I., Fallarero, A., Rosling, A., Khajeheian, M., Kolakovic, R., Genina, N., Nyman, J. and Vuorela, P., 2014. Towards fabrication of 3D printed medical devices to prevent biofilm formation. *International journal of pharmaceutics*, **459**(1-2), 62-64.
137. Water, J.J., Bohr, A., Boetker, J., Aho, J., Sandler, N., Nielsen, H.M. and Rantanen, J., 2015. Three-dimensional printing of drug-eluting implants: preparation of an antimicrobial polylactide feedstock material. *Journal of pharmaceutical sciences*, **104**(3), 1099-1107.
138. Chim, H., Hutmacher, D.W., Chou, A.M., Oliveira, A.L., Reis, R.L., Lim, T.C. and Schantz, J.T., 2006. A comparative analysis of scaffold material modifications for load-bearing applications in bone tissue engineering. *International journal of oral and maxillofacial surgery*, **35**(10), 928-934.
139. Holländer, J., Genina, N., Jukarainen, H., Khajeheian, M., Rosling, A., Mäkilä, E. and Sandler, N., 2016. Three-dimensional printed PCL-based implantable prototypes of medical devices for controlled drug delivery. *Journal of pharmaceutical sciences*, **105**(9), 2665-2676.
140. Genina, N., Holländer, J., Jukarainen, H., Mäkilä, E., Salonen, J. and Sandler, N., 2016. Ethylene vinyl acetate (EVA) as a new drug carrier for 3D printed medical drug delivery devices. *European Journal of Pharmaceutical Sciences*, **90**, 53-63.
141. Bhattacharjee, N., Urrios, A., Kang, S. and Folch, A., 2016. The upcoming 3D-printing revolution in microfluidics. *Lab on a Chip*, **16**(10), 1720-1742.
142. Zein, I., Hutmacher, D.W., Tan, K.C. and Teoh, S.H., 2002. Fused deposition modeling of novel scaffold architectures for tissue engineering applications. *Biomaterials*, **23**(4), 1169-1185.
143. Park, S.H., Park, D.S., Shin, J.W., Kang, Y.G., Kim, H.K., Yoon, T.R. and Shin, J.W., 2012. Scaffolds for bone tissue engineering fabricated from two different materials by the rapid prototyping technique: PCL versus PLGA. *Journal of Materials Science: Materials in Medicine*, **23**(11), 2671-2678.
144. Kim, J., McBride, S., Tellis, B., Alvarez-Urena, P., Song, Y.H., Dean, D.D., Sylvia, V.L., Elgendy, H., Ong, J. and Hollinger, J.O., 2012. Rapid-prototyped PLGA/β-TCP/hydroxyapatite nanocomposite scaffolds in a rabbit femoral defect model. *Biofabrication*, **4**(2), 025003.
145. Hennink, W.E. and Nostrum, Van C.F., 2012. Novel crosslinking methods to design hydrogels. *Advanced Drug Delivery Reviews*, **64**, 223-236.
146. Phillippi, J.A., Miller, E., Weiss, L., Huard, J., Waggoner, A. and Campbell, P., 2008. Microenvironments engineered by inkjet bioprinting spatially direct

adult stem cells toward muscle-and bone-like subpopulations. *Stem cells*, **26**(1), 127-134.

147. Billiet, T., Gevaert, E., De Schryver, T., Cornelissen, M. and Dubruel, P., 2014. The 3D printing of gelatin methacrylamide cell-laden tissue-engineered constructs with high cell viability. *Biomaterials*, **35**(1), 49-62.
148. Bertassoni, L.E., Cardoso, J.C., Manoharan, V., Cristino, A.L., Bhise, N.S., Araujo, W.A., Zorlutuna, P., Vrana, N.E., Ghaemmaghami, A.M., Dokmeci, M.R. and Khademhosseini, A., 2014. Direct-write bioprinting of cell-laden methacrylated gelatin hydrogels. *Biofabrication*, **6**(2), 024105.
149. Chinga-Carrasco, G., 2018. Potential and limitations of nanocelluloses as components in biocomposite inks for three-dimensional bioprinting and for biomedical devices. *Biomacromolecules*, **19**(3), 701-711.
150. Pfister, A., Landers, R., Laib, A., Hübner, U., Schmelzeisen, R. and Mülhaupt, R., 2004. Biofunctional rapid prototyping for tissue‐engineering applications: 3D bioplotting versus 3D printing. *Journal of Polymer Science Part A: Polymer Chemistry*, **42**(3), 624-638.
151. Murphy, C.A. and Collins, M.N., 2018. Microcrystalline cellulose reinforced polylactic acid biocomposite filaments for 3D printing. *Polymer Composites*, **39**(4), 1311-1320.
152. Pietrzak, K., Isreb, A., and Alhnan, M.A., 2015. A flexible-dose dispenser for immediate and extended release 3D printed tablets. *European Journal of Pharmaceutics and Biopharmaceutics*, **96**, 380-387.
153. Boetker, J., Water, J.J., Aho, J., Arnfast, L., Bohr, A. and Rantanen, J., 2016. Modifying release characteristics from 3D printed drug-eluting products. *European Journal of Pharmaceutical Sciences*, **90**, 47-52.
154. Chai, X., Chai, H., Wang, X., Yang, J., Li, J., Zhao, Y., Cai, W., Tao, T. and Xiang, X., 2017. Fused deposition modeling (FDM) 3D printed tablets for intragastric floating delivery of domperidone. *Scientific reports*, **7**(1), 2829.
155. Eqtesadi, S., Motealleh, A., Miranda, P., Lemos, A., Rebelo, A. and Ferreira, J.M., 2013. A simple recipe for direct writing complex 45S5 Bioglass® 3D scaffolds. *Materials Letters*, **93**, 68-71.
156. Kageyama, T., Osaki, T., Enomoto, J., Myasnikova, D., Nittami, T., Hozumi, T., Ito, T. and Fukuda, J., 2016. In situ cross-linkable gelatin-CMC hydrogels designed for rapid engineering of perfusable vasculatures. *ACS Biomaterials Science & Engineering*, **2**(6), 1059-1066.
157. Li, H., Tan, Y.J., Leong, K.F. and Li, L., 2017. 3D bioprinting of highly thixotropic alginate/methylcellulose hydrogel with strong interface bonding. *ACS applied materials & interfaces*, **9**(23), 20086-20097.
158. Kim, M. and Kim, G., 2015. 3D multi-layered fibrous cellulose structure using an electrohydrodynamic process for tissue engineering. *Journal of Colloid and Interface Science*, **457**, 180-187.
159. Pattinson, S.W. and Hart, A.J., 2017. Additive manufacturing of cellulosic materials with robust mechanics and antimicrobial functionality. *Advanced Materials Technologies*, **2**(4), 1600084.
160. Wang, Q., Sun, J., Yao, Q., Ji, C., Liu, J. and Zhu, Q., 2018. 3D printing with cellulose materials. *Cellulose*, **25**(8), 4275-4301.
161. Markstedt, K., Escalante, A., Toriz, G. and Gatenholm, P., 2017. Biomimetic inks

based on cellulose nanofibrils and cross-linkable xylans for 3D printing. *ACS applied materials & interfaces*, **9**(46), 40878-40886.
162. Akato, K., Tran, C.D., Chen, J. and Naskar, A.K., 2015. Poly (ethylene oxide)-assisted macromolecular self-Assembly of lignin in ABS matrix for sustainable composite applications. *ACS Sustainable Chemistry & Engineering*, **3**(12), 3070-3076.
163. Kai, D., Ren, W., Tian, L., Chee, P.L., Liu, Y., Ramakrishna, S. and Loh, X.J., 2016. Engineering poly (lactide)–lignin nanofibers with antioxidant activity for biomedical application. *ACS Sustainable Chemistry & Engineering*, **4**(10), 5268-5276.
164. Xu, C., Leppänen, A.S., Eklund, P., Holmlund, P., Sjöholm, R., Sundberg, K. and Willför, S., 2010. Acetylation and characterization of spruce (Picea abies) galactoglucomannans. *Carbohydrate research*, **345**(6), 810-816.
165. Saito, T., Nishiyama, Y., Putaux, J.L., Vignon, M. and Isogai, A., 2006. Homogeneous suspensions of individualized microfibrils from TEMPO-catalyzed oxidation of native cellulose. *Biomacromolecules*, **7**(6), 1687-1691.
166. Sundberg, A., Sundberg, K., Lillandt, C. and Holmbom, B., 1996. Determination of hemicelluloses and pectins in wood and pulp fibres by acid methanolysis and gas chromatography. *Nordic Pulp and Paper Research Journal*, **11**(4), 216-219.
167. Michielsen, S., 2003. Specific refractive index increments of polymers in dilute solution. The Wiley Database of Polymer Properties. DOI: 10.1002/0471532053.bra057.
168. Araki, J., Wada, M. and Kuga, S., 2001. Steric stabilization of a cellulose microcrystal suspension by poly (ethylene glycol) grafting. *Langmuir*, **17**(1), 21-27.
169. Liu, J., Korpinen, R., Mikkonen, K.S., Willför, S. and Xu, C., 2014. Nanofibrillated cellulose originated from birch sawdust after sequential extractions: a promising polymeric material from waste to films. *Cellulose*, **21**(4), 2587-2598.
170. Dixon, M.C., 2008. Quartz crystal microbalance with dissipation monitoring: enabling real-time characterization of biological materials and their interactions. J*ournal of biomolecular techniques: JBT*, **19**(3), 151.
171. Höök, F., Kasemo, B., Nylander, T., Fant, C., Sott, K. and Elwing, H., 2001. Variations in coupled water, viscoelastic properties, and film thickness of a Mefp-1 protein film during adsorption and cross-linking: a quartz crystal microbalance with dissipation monitoring, ellipsometry, and surface plasmon resonance study. *Analytical chemistry*, **73**(24), 5796-5804.
172. Tanase, C.E. and Spiridon, I., 2014. PLA/chitosan/keratin composites for biomedical applications. *Materials Science and Engineering: C*, **40**, 242-247.
173. Athanasiou, K.A., Niederauer, G.G., and Agrawal, C.M., 1996. Sterilization, toxicity, biocompatibility and clinical applications of polylactic acid/polyglycolic acid copolymers. *Biomaterials*, **17**(2), 93-102.
174. Schoultz, von S., Method for extracting biomass. 2015, WO2014009604A1.
175. Žepič, V., Poljanšek, I., Oven, P. and Čop, M., 2016. COST-FP1105: Properties of PLA films reinforced with unmodified and acetylated freeze dried nanofibrillated cellulose. *Holzforschung*, **70**(12), 1125-1134.
176. Wasanasuk, K. and Tashiro, K., 2011. Crystal structure and disorder in Poly (L-Lactic acid) δ form (α' form) and the phase transition mechanism to the

ordered α form. *Polymer*, **52**(26), 6097-6109.
177. Comb, J., Priedeman, W. and Turley, P.W., 1994. FDM® Technology process improvements. *In 1994 International Solid Freeform Fabrication Symposium*.
178. Leppiniemi, J., Lahtinen, P., Paajanen, A., Mahlberg, R., Metsä-Kortelainen, S., Pinomaa, T., Pajari, H., Vikholm-Lundin, I., Pursula, P. and Hytönen, V.P., 2017. 3D-printable bioactivated nanocellulose–alginate hydrogels. *ACS applied materials & interfaces*, **9**(26), 21959-21970.
179. Xu, C., Molino, B.Z., Wang, X., Cheng, F., Xu, W., Molino, P., Bacher, M., Su, D., Rosenau, T., Willför, S. and Wallace, G., 2018. 3D printing of nanocellulose hydrogel scaffolds with tunable mechanical strength towards wound healing application. *Journal of Materials Chemistry B*, **6**(43), 7066-7075.
180. Palaganas, N.B., Mangadlao, J.D., de Leon, A.C.C., Palaganas, J.O., Pangilinan, K.D., Lee, Y.J. and Advincula, R.C., 2017. 3D Printing of Photocurable Cellulose Nanocrystal Composite for Fabrication of Complex Architectures via Stereolithography. *ACS applied materials & interfaces*, **9**(39), 34314-34324.
181. Henriksson, I., Gatenholm, P., and Hägg, D., 2017. Increased lipid accumulation and adipogenic gene expression of adipocytes in 3D bioprinted nanocellulose scaffolds. *Biofabrication*, **9**(1), 015022.
182. Liu, Y. and Chan-Park, M.B., 2010. A biomimetic hydrogel based on methacrylated dextran-graft-lysine and gelatin for 3D smooth muscle cell culture. *Biomaterials*, **31**(6), 1158-1170.
183. O'Connell, C.D., Zhang, B., Onofrillo, C., Duchi, S., Blanchard, R., Quigley, A., Bourke, J., Gambhir, S., Kapsa, R., Di Bella, C. and Choong, P., 2018. Tailoring the mechanical properties of gelatin methacryloyl hydrogels through manipulation of the photocrosslinking conditions. *Soft matter*, **14**(11), 2142-2151.
184. Shin, S., Park, S., Park, M., Jeong, E., Na, K., Youn, H.J. and Hyun, J., 2017. Cellulose Nanofibers for the Enhancement of Printability of Low Viscosity Gelatin Derivatives. *BioResources*, **12**(2), 2941-2954.
185. Naseri, N., Poirier, J.M., Girandon, L., Fröhlich, M., Oksman, K. and Mathew, A.P., 2016. 3-Dimensional porous nanocomposite scaffolds based on cellulose nanofibers for cartilage tissue engineering: tailoring of porosity and mechanical performance. *RSC Advances*, **6**(8), 5999-6007.
186. Leppänen, A.S., Xu, C., Eklund, P., Lucenius, J., Österberg, M. and Willför, S., 2013. Targeted functionalization of spruce O-acetyl galactoglucomannans-2, 2, 6, 6‐tetramethylpiperidin-1-oxyl-oxidation and carbodiimide‐mediated amidation. *Journal of Applied Polymer Science*, **130**(5), 3122-3129.
187. Parikka, K., Leppanen, A.S., Pitkänen, L., Reunanen, M., Willfor, S. and Tenkanen, M., 2009. Oxidation of polysaccharides by galactose oxidase. *Journal of Agricultural and Food Chemistry*, **58**(1), 262-271.
188. Fukuoka, T., Uyama, H., and Kobayashi, S., 2004. Polymerization of polyfunctional macromolecules: synthesis of a new class of high molecular weight poly (amino acid) s by oxidative coupling of phenol-containing precursor polymers. *Biomacromolecules*, **5**(3), 977-983.
189. Kurisawa, M., Chung, J.E., Yang, Y.Y., Gao, S.J. and Uyama, H., 2005. Injectable biodegradable hydrogels composed of hyaluronic acid–tyramine conjugates for drug delivery and tissue engineering. *Chemical communications*, **34**, 4312-

4314.
190. Matsumoto, A., Ando, H., and Oiwa, M., 1989. Gelation in the copolymerization of methyl methacrylate with trimethylolpropane trimethacrylate. *European Polymer Journal*, **25**(4), 385-389.
191. Eckardt, N.A., 2008. Role of xyloglucan in primary cell walls. *The Plant Cell*, **20**, 1421–142.
192. Johansson, P., Brumer, H., Baumann, M.J., Kallas, Å.M., Henriksson, H., Denman, S.E., Teeri, T.T. and Jones, T.A., 2004. Crystal structures of a poplar xyloglucan endotransglycosylase reveal details of transglycosylation acceptor binding. *The Plant Cell*, **16**(4), 874-886.
193. Park, Y.B. and Cosgrove, D.J., 2015. Xyloglucan and its interactions with other components of the growing cell wall. *Plant and Cell Physiology*, **56**(2), 180-194.
194. Launey, M.E. and Ritchie, R.O., 2009. On the fracture toughness of advanced materials. *Advanced Materials*, **21**(20), 2103-2110.
195. Paluch, E.K., Nelson, C.M., Biais, N., Fabry, B., Moeller, J., Pruitt, B.L., Wollnik, C., Kudryasheva, G., Rehfeldt, F. and Federle, W., 2015. Mechanotransduction: use the force (s). *BMC biology*, **13**(1), 47.
196. Han, F., Zhu, C., Guo, Q., Yang, H. and Li, B., 2016. Cellular modulation by the elasticity of biomaterials. *Journal of Materials Chemistry B*, **4**(1), 9-26.
197. Butcher, D.T., Alliston, T., and Weaver, V.M., 2009. A tense situation: forcing tumour progression. *Nature Reviews Cancer*, **9**(2), 108.
198. Kyle, S., Jessop, Z.M., Al‐Sabah, A. and Whitaker, I.S., 2017. 'printability'of Candidate Biomaterials for Extrusion Based 3d Printing: State-of-the-art. *Advanced healthcare materials*, **6**(16), 1700264.
199. Nichol, J.W., Koshy, S.T., Bae, H., Hwang, C.M., Yamanlar, S. and Khademhosseini, A., 2010. Cell-laden microengineered gelatin methacrylate hydrogels. *Biomaterials*, **31**(21), 5536-5544.
200. Liu, J., Cheng, F., Grénman, H., Spoljaric, S., Seppälä, J., Eriksson, J.E., Willför, S. and Xu, C., 2016. Development of nanocellulose scaffolds with tunable structures to support 3D cell culture. *Carbohydrate polymers*, **148**, 259-271.
201. Kumari, S., Vermeulen, S., van der Veer, B., Carlier, A., de Boer, J. and Subramanyam, D., 2018. Shaping Cell Fate: Influence of Topographical Substratum Properties on Embryonic Stem Cells. *Tissue Engineering Part B: Reviews*, **24**(4), 255-266.
202. Lutolf, M.P., Gilbert, P.M. and Blau, H.M., 2009. Designing materials to direct stem-cell fate. *Nature*, **462**(7272), 433.
203. Murphy, C.M. and O'Brien, F.J., 2010. Understanding the effect of mean pore size on cell activity in collagen-glycosaminoglycan scaffolds. *Cell adhesion & migration*, **4**(3), 377-381.

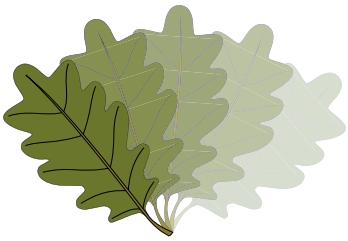

Johan Gadolin
Process Chemistry Centre

ISBN 978-952-12-3788-1